Research Square

Preprints are preliminary reports that have not undergone peer review.
They should not be considered conclusive, used to inform clinical practice,
or referenced by the media as validated information.

Comparative multi-omics of host genome, metabolome and associated rhizosphere microbiota across karst-endemic and widespread Rhododendron species

Sulin Wen
Guizhou University
Yuxin Leng
Guizhou University
Hulan Yao
Guizhou University
Kui Zhou
Guizhou University
Yi Min
Guizhou University
Lei Peng
Guizhou University
Jing Ou
Guizhou University
Guang Qiao
Guizhou University
Xiaopeng Wen
Guizhou University
Guijie Ding
gjding@gzu.edu.cn
Guizhou University

Research Article

Keywords: Karst adaptation, Multi-omics, Plant–microbiome interactions, Rhizosphere microbiome, Rhododendron, Secondary metabolites

Posted Date: November 4th, 2026

DOI: https://doi.org/10.21203/rs.3.rs-11199507/v1

License: This work is licensed under a Creative Commons Attribution 4.0 International License. Read Full License

Additional Declarations: No competing interests reported.

Abstract

Background

To examine how classically calcifuge plants persist in phosphorus-poor, high-Ca^{2+} karst bare-rock habitats, we compared genome, leaf-metabolome and associated rhizosphere-microbiome patterns in the karst-endemic *Rhododendron bailiense* Y.P.Ma, C.Q.Zhang & D.F.Chamb. with those in the widespread *R. delavayi* Franch. and allopatric *R. ambiguum* Hemsl. We integrated a multi-omics investigation across three natural microhabitats to decode these inter-kingdom interactions, combining whole-genome comparative analysis, UHPLC-MS/MS non-targeted leaf metabolomics, fungal internal transcribed spacer (ITS) amplicon profiling, and deep rhizosphere metagenomic sequencing.

Results

Comparative genomics revealed significant expansion of secondary metabolism gene families in *R. bailiense*. Metabolomics showed a distinct chemical profile rich in specific flavonoids and polyacetylenes, such as luteolinidin and safynol. These species-specific metabolite profiles co-varied with microbial hubs, including *Piloderma*, *Streptomyces*, *Pseudorhodoplanes* and *Candidatus Sulfotelmatobacter*, whose reported or predicted functions are relevant to phosphorus mobilization, rhizosphere defence, recalcitrant-carbon turnover and mineral-associated sulfur cycling. In contrast, the *R. delavayi* and *R. ambiguum* rhizospheres were enriched in saprotrophic taxa, including *Mortierella*, consistent with broader nutrient-turnover potential.

Conclusions

R. bailiense showed a species-specific leaf-metabolite profile that co-varied with a distinctive rhizosphere microbiome. Together, these coordinated patterns suggest a potential functional link between species-specific host chemistry and rhizosphere-community organization, and highlight microbial and metabolic candidates relevant to karst persistence and conservation.

Background

It is not only a plant that evolves but also the microbes and microbes living within form a highly integrated evolutionary and ecological unit, which is termed 'Holobiont' [1, 2]. In the network of diverse interactions, the rhizosphere operates as a significant microdomain of material and information exchange between plants and soil organisms. Contemporary microbial-ecology frameworks view the plant-associated microbiome as a potential component of the host extended phenotype [3, 4]. Such associations can influence host responses to abiotic stress, nutrient acquisition and pathogen pressure. The recently proposed Functional Team Selection (FTS) framework suggests that, under strong environmental stress or resource limitation, host traits and local environmental filtering may favour microbial assemblages with functions complementary to host resource acquisition or stress tolerance [5]. However, current research on the mechanisms of microbial community assembly and functional compensation has largely focused on model crop systems. The operation of these cross-boundary co-evolutionary rules in wild, non-domesticated plant populations subjected to extreme environmental filtering remains a significant frontier gap in the field of evolutionary ecology.

Karst landforms represent one of the most challenging terrestrial ecosystems for plant survival on Earth, characterized by shallow and discontinuous soils, recurrent drought, exposed rock surfaces and high calcium availability associated with carbonate parent material [6–8]. For the genus *Rhododendron*, which boasts a vast species diversity, colonizing karst habitats presents a significant evolutionary paradox. Most *Rhododendron* species are typical acidophilic plants and are calcium-intolerant; they often suffer from iron chlorosis and osmotic imbalance in carbonate-rich soils [9]. However, narrow-endemic species such as *Rhododendron bailiense* Y.P.Ma, C.Q.Zhang & D.F.Chamb. survive on the harsh karst bare rock summits of southwest China [10]. Recent high-quality genomic studies over the past two years have indicated that *R. bailiense* has developed a fundamental genetic basis for coping with high calcium stress by expanding gene families related to calcium ion transport (such as Ca^{2+}-ATPase) and detoxification (such as cytochrome P450) [11, 12]. However, in the face of a phosphorus-poor, high-Ca^{2+} bare-rock environment, structural variation of the host genome alone may be insufficient to sustain ecological success. This raises a fundamental question: to what extent might the persistence of karst-endemic species be associated with the assembly of functionally specialized rhizosphere microbial communities?

The classic niche theory posits that sympatric species must achieve niche differentiation to avoid competitive exclusion. Recent studies have shown that, although the rhododendron community exhibits phylogenetic or functional convergence, the dissimilarity in fungal community composition and the high level of network specialization facilitate the coexistence of rhododendrons [13]. Therefore, we hypothesize that the evolutionary trajectories of the highly specialized narrow-endemic species, *R. bailiense*, and its closely distributed,

ecologically plastic widespread species, *R. delavayi* Franch., diverge not only in their aboveground parts but also profoundly reflect in the underground micro-ecosystem. Research indicates that widespread species tend to adopt a 'generalist' microbial assembly strategy, constructing open and highly connected networks to achieve broad environmental tolerance; in contrast, endemic species in extreme environments may adopt a 'specialist' strategy, being associated with a more restricted core microbial community that may contribute to persistence in specific microhabitats [14].

Plant secondary metabolism is believed to be a potential link between host genetic identity and rhizosphere-community assembly [15]. Plant communities employ a great deal of photosynthetically fixed carbon for the synthesis of complex secretions and metabolic molecules. These molecules act as carbon sources for microorganisms, which enhances nutrient cycling. In particular, they interact with specific microorganisms. Therefore, they act as “chemical communication signals” and “ecological filters” [3, 16]. Recent multi-omics studies suggest that particular secondary metabolites can influence the chemotaxis and colonization of rhizosphere microorganisms. For example, various flavonoids, such as Luteolinidin, utilize their structural features as potent chemotactic agents for beneficial bacteria including *Bacillus* [15]. Similarly, polyacetylenes, such as Safynol, and ketone derivatives act as potent chemical filters, potentially suppressing sensitive microorganisms, including some pathogens and saprotrophs [17]. Given the conservation and methodological constraints on destructive root sampling of karst-endemic species in fragile rock crevices, leaf metabolomics provides a non-destructive view of species-specific host chemistry, while not establishing which compounds are transported to roots or released into the rhizosphere.

Building on this background, we designed an integrated multi-omics study (comparative genomics, non-targeted metabolomics, fungal ITS profiling, and deep metagenomic sequencing) of representative *Rhododendron* species: the karst-endemic *R. bailiense* (Rb), the widespread *R. delavayi* (Rd), and *R. ambiguum* Hemsl. (Ram) from a contrasting acidic-soil habitat (leaf metabolomics additionally included *R. decorum* Franch.). We address two questions: (1) How do the rhizosphere microbial communities of these ecologically distinct *Rhododendron* species differ in composition and functional potential? (2) Are these microbial differences mirrored by distinct host genomic and chemical profiles, pointing to a coordinated host–microbiome signature of karst adaptation? By addressing these questions, we characterize patterns of co-variation among host genome, secondary metabolites and the rhizosphere community, and propose testable hypotheses relevant to the conservation of small karst-endemic populations and to plant resilience under climate change.

Methods

Site selection and sample collection

To investigate adaptive divergence of *Rhododendron* across contrasting edaphic settings, we sampled four species spanning three microhabitats in two regions of subtropical southwestern China. Three taxa, *R. bailiense*, *R. delavayi* and *R. decorum*, occur within a single protected landscape, the Baili *Rhododendron* Nature Reserve (BRNR; Bijie, Guizhou): *R. bailiense* on exposed karst summits in Yongxing Village (27°14'24"N, 105°52'42"E), and the co-occurring *R. delavayi* and *R. decorum* in an adjacent yellow-soil stand (27°13'43"N, 105°51'55"E). *R. ambiguum* was sampled at Wawu Mountain (Meishan, Sichuan; 29°38'50"N, 102°56'33"E), a geographically proximate site within the same subtropical monsoon climate belt. Each species was sampled from *Rhododendron*-dominated stands largely free of other woody plants, so that confounding of the rhizosphere community by co-occurring non-host vegetation was minimized. All individuals were collected within a single week in early May (5–11 May 2025), minimizing phenological and seasonal variation among samples.

The three habitats differed in parent material and soil development. *R. bailiense* occupied exposed karst summits, where a thin, discontinuous humus layer accumulated in rock crevices over limestone/dolomite amid high rock exposure and recurrent drought. *R. delavayi* and co-occurring *R. decorum* grew in better-developed mountain yellow soil, whereas *R. ambiguum* occupied deep yellow-brown soil on basalt-dominated silicate parent material at Wawu Mountain.

From three healthy adult individuals per species (≥ 5 m apart), we collected rhizosphere soil and corresponding fully expanded mature leaves following aseptic protocols for microbiome sampling. Because the karst substrate is shallow and rocky, intact root systems were generally difficult to recover; we therefore profiled root-zone (rhizosphere) soil rather than root tissue. At each plant, loose soil was removed, and the soil associated with the root zone was retained and immediately flash-frozen in liquid nitrogen together with the leaf samples before storage at − 80°C. Omics coverage was tailored to genome availability and habitat representation: comparative genomics focused on the two species with high-quality reference genomes and the strongest habitat contrast (*R. bailiense* vs *R. delavayi*; Additional file 1: Fig. S1); rhizosphere fungal ITS amplicon and shotgun metagenomic profiling covered the three species representing the three microhabitats (*R. bailiense*, *R. delavayi*, *R. ambiguum*); and leaf metabolomics included all four species, with *R. decorum* added as a same-site, same-habitat reference for *R. delavayi* to separate species-level metabolic variation from habitat effects. Because no rhizosphere microbiome data were generated for *R. decorum*, it contributed only to cross-species metabolite comparisons and was excluded from all metabolite–microbiome analyses.

The plant material used in this study was formally identified by one of the authors, Sulin Wen (Guizhou University), on the basis of diagnostic morphological characters and by comparison with authenticated reference specimens held in public herbaria and accessible through the Chinese Virtual Herbarium (CVH; https://www.cvh.ac.cn/): *Rhododendron bailiense* Y.P.Ma, C.Q.Zhang & D.F.Chamb. (KUN 1550524; Herbarium, Kunming Institute of Botany, Chinese Academy of Sciences [KUN]), and *R. delavayi* Franch. (PE 02110190), *R. ambiguum* Hemsl. (PE 00266961) and *R. decorum* Franch. (PE 02283857) (Chinese National Herbarium, Institute of Botany, Chinese Academy of Sciences [PE]). These herbarium sheets served only as reference material for identification and are not vouchers of the individuals sampled here. Voucher specimens of the sampled individuals were not prepared and have therefore not been deposited in a public herbarium.

Soil physicochemical analyses

For habitat-level edaphic characterization, three soil samples were analysed per habitat. Air-dried soils were sieved, and concentrations were expressed on an oven-dry mass basis. Soil organic matter was determined by dichromate-sulfuric acid oxidation and $FeSO_4$ back-titration; total N by Kjeldahl digestion followed by continuous-flow colorimetry; and total P by NaOH fusion and molybdenum-antimony colorimetry. Alkali-hydrolyzable N was measured by alkaline diffusion. Available P was extracted with 0.5 mol L^{-1} $NaHCO_3$ (pH 8.5) and quantified colorimetrically. Available S was operationally assessed from sulfate in a 1:5 soil-to-water extract by $BaCl_2$ precipitation and EDTA back-titration. Exchangeable Ca^{2+} was extracted with 1 mol L^{-1} ammonium acetate (pH 7.0) and quantified by EDTA complexometric titration. Soil pH was measured potentiometrically in a 1:2.5 soil-to-water suspension.

Comparative genomics analysis

To elucidate the genetic basis of *R. bailiense* adaptation to extreme karst habitats, we systematically compared its genome with that of the co-distributed *R. delavayi*. Whole-genome alignment was performed using SyRI v1.6.3 [18] to identify structural variations (inversions, translocations and duplications) and retrieve unaligned, taxon-specific regions. We then reconstructed phylogenetic relationships and analyzed gene-family expansions and contractions to identify lineage-specific genomic changes. Finally, GO and KEGG enrichment analyses were performed on expanded and taxon-specific genes to identify potential adaptive mechanisms, including secondary-metabolite biosynthesis and environmental signal transduction. Additional details regarding genomic data sources, bioinformatic pipelines and software parameters are provided in Additional file 2: Note S1.

ITS sequencing and data processing of rhizosphere fungi

Using the DNeasy PowerSoil Pro Kit (QIAGEN, Germany), total genomic DNA was extracted from frozen rhizosphere soil samples. The lysis system of this kit is optimized to eliminate humic acids and the heavy metal inhibitors that are common in karst soils to obtain high-purity microbial DNA. The NanoDrop 2000 UV spectrophotometer and 1% agarose gel electrophoresis were used to assess DNA quality. Universal primers ITS1F/ITS2R were used to amplify the ribosomal internal transcribed spacer (ITS) region for fungal-community analysis. Sequencing was performed on the Illumina NovaSeq 6000 platform. The resulting sequences were imported into the QIIME 2 workflow [19], where strict quality filtering, denoising and chimera removal were conducted using the DADA2 plugin [20] to generate an amplicon sequence variant (ASV) feature table. ASVs were taxonomically classified using the classify-sklearn algorithm [21] against the UNITE 9.0 database [22] (confidence threshold, 70%). After mitochondrial and chloroplast contaminant sequences were removed, sample abundances were standardized to account for differences in sequencing depth. For more detailed instructions, please refer to Additional file 2: Note S2.

Metagenomic sequencing and functional annotation

To comprehensively analyze the functional potential of rhizosphere prokaryotes (particularly in relation to C, N, P, and S cycles and stress resistance genes), we performed deep metagenomic sequencing (using the Illumina NovaSeq platform) on nine rhizosphere soil DNA samples, yielding a total of approximately 60 Gb of raw data. First, raw reads were quality-controlled and filtered using fastp (v0.20.0) [23] to remove low-quality bases and adapter sequences. The resulting high-quality clean reads were subjected to de novo assembly using MEGAHIT (v1.2.9) [24], with contigs shorter than 500 bp filtered out. Prodigal (v2.6.3) [25] was used to predict open reading frames (ORFs, ≥ 100 bp), which were then clustered using CD-HIT (v4.6.1) [26] under the criteria of ≥ 95% sequence identity and ≥ 90% coverage to construct a non-redundant gene set. SOAPaligner (v2.21) [27] was used to map high-quality reads from each sample back to the non-redundant gene set and calculate gene abundance (TPM). For functional and taxonomic annotation, DIAMOND (v2.0.13) [28] was used to align translated non-redundant gene sequences against the NR database for taxonomic assignment and against the KEGG, ARDB, CARD and VFDB databases (E value ≤ 1 × 10 − 5) to profile pathways related to biogeochemical cycles, two-component systems and chemotaxis. For more detailed instructions, please refer to Additional file 2: Note S3.

Non-targeted metabolomics analysis of leaves

To characterize host-level chemistry and explore species-specific metabolites that might be associated with the rhizosphere microbiome, we performed non-targeted metabolomic profiling of *Rhododendron* leaves using ultra-high-performance liquid chromatography–high-resolution mass spectrometry (UHPLC-MS/MS). Leaf metabolomics included four species (*R. bailiense*, *R. delavayi*, *R. ambiguum* and *R. decorum*). *R. decorum*, which co-occurs with *R. delavayi* in the same yellow-soil habitat, was included as an additional same-habitat reference to separate species-level metabolic variation from habitat-level effects; because no rhizosphere microbiome data were generated for *R. decorum*, it was excluded from all metabolite–microbiome integration analyses, which were restricted to the three species with paired microbiome data.

We profiled leaves rather than roots for several practical and conservation-related reasons. Although root-derived secondary metabolites are most directly informative about metabolite–microbe interactions in the rhizosphere, the focal species are protected and, in the case of *R. bailiense*, rare; we therefore avoided the destructive root excavation that comprehensive root metabolomics would require. In addition, many root secondary metabolites are biosynthesized in the leaves and transported belowground, so the leaf metabolome reflects a large part of each species' characteristic secondary-metabolite repertoire, even though whether specific compounds are ultimately enriched in roots remains to be determined. Finally, our current root-sampling and cleaning procedures did not yet yield root material of sufficient quantity and purity for reliable metabolomic analysis; refining these protocols is ongoing work. We therefore use the leaf metabolome here as a practical proxy for species-specific host chemistry, to examine its potential associations with co-occurring rhizosphere microbes, while recognizing that direct characterization of root secondary metabolites and their interactions with the rhizosphere microbiome is an important direction for future work.

Sample preparation included standardized steps such as ultrasonic extraction, centrifugation, and resuspension [29]. Chromatographic separation was performed on a Thermo Fisher UHPLC-Q Exactive HF-X system equipped with an ACQUITY UPLC HSS T3 column (100 mm × 2.1 mm, 1.8 μm). Mobile phase A consisted of an aqueous solution containing 0.1% formic acid (with 5% acetonitrile), and mobile phase B consisted of a mixed organic solvent containing 0.1% formic acid (47.5% acetonitrile + 47.5% isopropanol + 5% water). Mass spectrometry was performed in positive/negative ion electrospray ionization (ESI) mode with data-dependent acquisition (DDA), with the Orbitrap mass analyzer resolution set to 60,000 and a scan range of 70–1050 m/z. Raw data files were imported into Progenesis QI (v2.3, Waters) for peak alignment and peak extraction. Metabolites were cross-validated and deeply annotated using secondary mass spectrometry (MS/MS) data from the Majorbio internal database, Metlin, and HMDB. Partial least squares discriminant analysis (PLS-DA) was performed using the R package ropls. The strict selection criteria for differential metabolites (DMs) were Variant Importance in Projection (VIP) > 1.0 and $P < 0.05$ [30]. For more detailed information and weighted gene co-expression network analysis (WGCNA) analysis, please refer to Additional file 2: Note S4.

Multi-omics integration and statistical analysis

All bioinformatics and statistical analyses were conducted using the Majorbio Cloud online platform (https://cloud.majorbio.com) and R language (v4.2.2). For diversity and differential analyses, alpha-diversity indices (ACE, Chao1, Shannon, Simpson) were calculated using Mothur (v1.30.2) [31] and R. Principal coordinates analysis (PCoA) was used to visualize between-group differences. The Kruskal-Wallis H test or Wilcoxon rank-sum test combined with LEfSe analysis [32] (LDA threshold > 2.0) was used to identify characteristic fungal and bacterial groups driving habitat differentiation. Functional predictions from the fungal amplicon data were generated with PICRUSt2 [33], and ecological guild assignments were obtained with FUNGuild [34]. For multi-omics association analysis, WGCNA [35] was applied to the non-targeted leaf-metabolomic data to identify species-associated chemical modules. Metabolites with high VIP rankings in these modules, including safynol and luteolinidin, were then tested by Spearman rank correlation against core microbial genera, including *Piloderma*, *Bradyrhizobium*, that differed significantly in the metagenomic data. Statistical graphics and networks were generated using ggplot2 and Cytoscape v3.9.1, respectively.

Results

Distinct habitats and divergent genomic features among Rhododendron species

The adaptation of plants to extreme habitats is often linked to genomic specialization. Here, we examined three typical *Rhododendron* habitats across the Baili *Rhododendron* Nature Reserve (Guizhou) and Wawu Mountain (Sichuan) (Fig. 1A, B). The habitats differed in all measured soil properties (Welch's ANOVA, $P \leq 0.012$; Fig. 1D–K), revealing distinct nutrient profiles. The *R. bailiense* habitat combined the highest soil organic matter and total N with the highest exchangeable Ca^{2+}. Its total and available P were both lower than those in the *R. ambiguum* habitat, whereas only available P did not differ significantly from the low value in the *R. delavayi* habitat. Thus, despite its shallow karst setting, the *R. bailiense* habitat was not uniformly nutrient-poor: its thin humus soil contained abundant organic matter and N, but

remained P-poor and high in exchangeable Ca^{2+}. The *R. delavayi* habitat was likewise P-poor and had the lowest soil organic matter, total N, alkali-hydrolyzable N and available S. By contrast, the *R. ambiguum* habitat had the highest total P, available P, alkali-hydrolyzable N and available S, while retaining intermediate soil organic matter and total N. Exchangeable Ca^{2+} was lower in the *R. delavayi* and *R. ambiguum* habitats than in the *R. bailiense* habitat, but remained at moderate levels in both. All three soils were acidic; pH was highest in the *R. bailiense* habitat, intermediate in the *R. delavayi* habitat and lowest in the *R. ambiguum* habitat. Together, these habitats spanned a pronounced edaphic gradient from a karst summit rich in organic matter, N and Ca^{2+} but poor in P, through a comparatively nutrient-poor and P-poor yellow-soil habitat, to a yellow-brown soil relatively rich in P, alkali-hydrolyzable N and S. This habitat heterogeneity is consistent with the divergent environmental adaptation strategies these species may have followed over their evolutionary history.

To elucidate niche differentiation from a genetic perspective, we conducted whole-genome synteny and structural-variation analysis between the endemic *R. bailiense* and the widespread *R. delavayi* using published high-quality genomes (Fig. 1C; Additional file 3: Table S1). Although the two species shared some categories of genes enriched in their non-aligned regions (both involving secondary-metabolic processes), *R. bailiense* contained a larger absolute number of stress-related and metabolic genes (Additional file 1: Fig. S3A, B). This difference is mirrored in their gene-family histories: at its terminal branch, *R. bailiense* showed a pronounced gene-family expansion (1,940 families expanded, versus 823 in *R. delavayi*; Additional file 1: Fig. S2), representing a large genetic reservoir potentially relevant to its extreme karst habitat (Additional file 1: Fig. S3E, F). Notably, this expansion was also markedly greater than that of its close relative *R. liliiflorum* (Additional file 1: Fig. S2). The lineage-specific nature of this expansion suggests that the genomic features associated with *R. bailiense*'s habitat are not simply shared across its close relatives, consistent with the dynamic, lineage-specific gene-family evolution evident across *Rhododendron* (Additional file 1: Fig. S2).

In-depth analysis showed that the non-aligned regions of *R. bailiense* were enriched in pathways for "Biosynthesis of other secondary metabolites," "Metabolism of terpenoids and polyketides," and "Plant–pathogen interaction" (Additional file 1: Fig. S3A). This substantial secondary-metabolite capacity may support both physiological defence against karst stress and the production of chemical signals with potential relevance to rhizosphere community assembly. The enrichment of plant–pathogen-interaction annotations further points to defence perception and signalling as a possible component of survival under recurrent karst stress. Together with expanded secondary-metabolism capacity, this pattern suggests a coordinated chemical and immune repertoire that may support physiological defence and influence nearby microbes. Although *R. delavayi* shared broadly similar gene categories, the abundance of these genes was lower; its non-aligned regions were instead enriched in phenylpropanoid and flavonoid biosynthesis pathways (Additional file 1: Fig. S3B). These compounds are well-known mediators of plant–microbe signalling, and their enrichment in *R. delavayi* may reflect a species- and habitat-associated chemical repertoire. Detailed analyses of gene-family expansions and metabolic-transport functions are provided in Additional file 2: Note S5.

Host- and habitat-associated differentiation of rhizosphere fungal communities

The evolutionary divergence of host genomes is often accompanied by the restructuring of subterranean micro-ecosystems. To elucidate this process, we assessed the assembly patterns of rhizosphere fungi associated with three species of *Rhododendron* through fungal ITS amplicon sequencing (Additional file 3: Table S2; Additional file 4). PCoA analysis revealed significant differences in the fungal composition of the rhizospheres of the three *Rhododendron* species (Fig. 2A). The Alpha diversity indices (ACE, Sobs, and Chao) of the mycorrhizal fungi in the rhizospheres of *R. bailiense* and *R. delavayi* were slightly higher than those of *R. ambiguum* (Fig. 2B, C; Additional file 1: Fig. S4C; Additional file 3: Table S3), reflecting a slight advantage in the number of fungal species in the former two rhizospheres. However, the Shannon index of *R. bailiense* was slightly lower than that of the other two species, while the Simpson index was slightly higher, indicating a marginally lower diversity of rare and dominant species. Notably, the dominant microbial community structures of the three types of rhododendrons exhibit distinctly different characteristics (Fig. 2D): the most dominant genus in the rhizosphere of *R. bailiense* is *Piloderma*, while *R. delavayi* and *R. ambiguum* share *Mortierella* as the dominant genus. A comparative analysis of the proportions of various fungal genera also reflects the differences in the composition of rhizosphere fungi among the three types of rhododendrons (Fig. 2D). Furthermore, we investigated the composition of rhizosphere fungi in the three *Rhododendron* types through the visualization of the LEfSe species hierarchy tree (Fig. 2E). The results further reveal that the three fungal groups have formed their respective dominant fungal communities. For instance, the dominant fungal community in the rhizosphere of *R. bailiense* belongs to the phylum *Basidiomycota*, whereas the dominant fungal community in the rhizosphere of *R. delavayi* belongs to the phyla *Ascomycota* and Mortierellomycota. These results show distinct fungal-community composition among the three *Rhododendron* rhizospheres.

To further analyze community differences from a phylogenetic perspective, we constructed a phylogenetic tree of core fungal genera (Fig. 3A). The rhizosphere fungal communities of different *Rhododendron* species showed marked phylogenetic clustering and host association. For instance, *Gorgomyces* and *Phaeothecoidea* were largely confined to the *R. delavayi* rhizosphere and nearly absent from the other two. *Piloderma* was strongly enriched in the *R. bailiense* rhizosphere, whereas *Mortierella* was enriched in those of *R. delavayi* and *R.*

ambiguum; the abundance of these genera greatly exceeded that of others, suggesting they are dominant members of their respective communities. Kruskal–Wallis H tests confirmed species-associated differences in the abundance of specific fungal genera; for example, *Piloderma*, *Mycena*, *Podila* and *Trichoderma* were enriched in the *R. bailiense* rhizosphere (Fig. 3D; Additional file 1: Fig. S5), and such differences were also evident at the phylum level (Additional file 1: Fig. S6B). The *R. bailiense* rhizosphere contained proportionally more generalist and fewer specialist taxa (Fig. 3C; Additional file 1: Fig. S6A), indicating a lower richness of rare fungal taxa than in *R. delavayi* and *R. ambiguum*, consistent with its Shannon index. The strong association between *R. bailiense* and *Piloderma* identifies this genus as a candidate fungal partner and is consistent with host selection, habitat filtering or their joint action in the karst habitat. The enrichment of *Mortierella, a widespread generalist saprotroph active in carbon and nutrient turnover, in R. delavayi* and *R. ambiguum* is in line with the broader habitats of these two widely distributed species.

Furthermore, analysis of fungal functional guilds revealed differences among the three rhizosphere communities (Fig. 3B). The proportion of saprotrophic fungi was highest in the *R. delavayi* rhizosphere, whereas ectomycorrhizal fungi predominated in that of *R. bailiense*, pointing to contrasting nutritional strategies between the two. The enrichment of ectomycorrhizal fungi, including *Piloderma*, in the *R. bailiense* rhizosphere is notable because such fungi can, through their fine hyphae, penetrate rock microfractures and secrete phosphatases to mobilize bound phosphorus. Several enzyme-coding functions enriched in the *R. bailiense* rhizosphere are consistent with this nutritional context (Fig. 3E): acid phosphatase, which could contribute to mobilizing insoluble phosphorus in rock-crevice habitats; chitinase and β-glucosidase, indicating potential for organic-matter decomposition and carbon turnover; and glutathione transferase and aldehyde dehydrogenase, associated with detoxification capacity. Together, these results indicate that the rhizosphere fungal communities of the three *Rhododendron* species differ in both phylogenetic composition and functional guild structure in a host-associated manner, and that the *R. bailiense* community is enriched in functional potentials relevant to phosphorus mobilization, organic-matter turnover and stress-associated processes in its karst habitat.

Distinct prokaryotic community composition and functional potential across species

Given that the rhizosphere fungal communities of *Rhododendron* showed strong host-associated differentiation, we asked whether the broader rhizosphere community, particularly dominant bacterial and archaeal taxa, differed correspondingly in functional potential. To address this, we performed deep metagenomic sequencing of rhizosphere soils from three *Rhododendron* species (Additional file 3: Tables S4–S9; Additional file 5). Taxonomic annotation of the non-redundant gene set showed that the prokaryotic communities of *R. bailiense*, *R. delavayi* and *R. ambiguum*, like the fungal communities, separated clearly along host identity (Fig. 4B; Additional file 1: Fig. S7D). *R. bailiense* consistently showed the lowest alpha diversity across multiple indices *(*Fig. 4A, C, D; *Additional file 1: Fig. S7A–C; Additional file 3: Table S10)*, coinciding with its distinctive high-Ca^{2+}, P-poor karst-soil context. This pattern is consistent with strong environmental filtering, host-associated effects or their joint action, and motivates future paired bulk-soil comparisons.

Metagenomic assembly and annotation yielded 3,076,709 predicted genes (Additional file 3: Table S8), most of which were 201–800 bp long (Fig. 4E). NR, COG and KEGG yielded the largest annotated gene sets (Additional file 1: Fig. S8A), with carbohydrate metabolism, amino-acid metabolism and signal transduction among the predominant functional categories (Fig. 4F; Additional file 1: Fig. S8B). At genus level, the three rhizospheres were dominated by Proteobacteria and Actinobacteriota, with both phyla proportionally more abundant in *R. bailiense* (Fig. 4G), consistent with strong dominance by a narrower set of taxa. The three groups shared 2,441 taxa, whereas 183 taxa were detected only in the *R. bailiense* group, defining a group-specific candidate pool (Fig. 4I). Genus-level associations are summarized in Additional file 1: Fig. S9. KEGG level-3 annotation further showed high representation of biosynthesis of secondary metabolites and two-component systems (Fig. 4H). Thus, the three host-habitat groups contained taxonomically distinct assemblages with substantial functional overlap (Fig. 4J).

In addition, LDA (Linear Discriminant Analysis) was performed to identify the specific metabolic pathways characteristic of the various groups (Fig. 5A). The results indicated that the rhizosphere microorganisms in various habitats displayed distinct functional profiles: the *R. bailiense* rhizosphere was significantly enriched in bacterial chemotaxis, flagellar assembly, and fatty acid biosynthesis. Notably, the high abundance of chemotaxis and flagellar-assembly genes suggests that the *R. bailiense* rhizosphere is enriched in microbial taxa with the potential for motility and active foraging in karst rock fissures, where moisture is highly unstable and nutrients are spatially heterogeneous; the enrichment of fatty-acid-biosynthesis pathways is consistent with membrane-related functions that may be relevant under high-Ca^{2+} and drought-prone conditions. The widespread species (*R. delavayi*) exhibited a 'high-efficiency turnover' strategy: the rhizosphere of *R. delavayi* displayed exceptionally high abundances of ABC transporters and metabolism of alanine, aspartate, and glutamate. This profile is consistent with microbial transformation and uptake of limited carbon and nitrogen pools in the *R. delavayi* habitat, which had the lowest soil organic matter, total N and alkali-hydrolyzable N. The *R. ambiguum* rhizosphere was distinguished by higher abundance of genes assigned to biofilm formation (biofilm formation - *Pseudomonas aeruginosa*) and meiosis (meiosis - yeast) pathways. These annotations suggest greater potential for surface-associated community formation and interspecies signalling in its yellow-brown soil context.

The clustering heatmap based on the top 30 KEGG pathway abundances (Fig. 5B) further revealed distinct functional profiles among the three *Rhododendron* rhizospheres. *R. delavayi* showed higher representation of pathways related to carbon metabolism and amino-acid biosynthesis, consistent with microbial potential for carbon and nitrogen turnover in the yellow-soil habitat. In contrast, pathways with higher gene abundance in *R. bailiense* included benzoate and aromatic-compound degradation. This enrichment suggests microbial potential for complex-organic-matter turnover and nominates these substrates for direct process measurements. *R. ambiguum* showed fewer high-abundance pathways among the selected set, consistent with a distinct functional allocation. Furthermore, by integrating the dominant groups from three types of rhizosphere soils (Fig. 5C) with the abundance heatmap of the top 50 core genera (Fig. 5D), it was found that core species underwent a complete turnover in different habitats. *R. delavayi* significantly enriched typical aerobic saprophytic bacteria such as *Mehceanibacter* and *Luteitalea*, which specialize in organic matter degradation in deep yellow soil. Notably, dominant genera in the *R. bailiense* rhizosphere included *Bradyrhizobium* and *Candidatus Sulfotelmatobacter*. Their abundance, together with group-level nutrient-cycling annotations, identifies candidate roles in oligotrophic persistence, plant association and mineral-associated processes.

The Circos diagrams simultaneously display the distribution between taxa and functions (Fig. 5E, F). In taxonomic composition (Fig. 5E), the *R. bailiense* rhizosphere was enriched in phyla such as *Pseudomonadota* and *Acidobacteriota*, which are often associated with tolerance of environmental stress. Despite differences in the taxa enriched across the three species, their core functions were concentrated in shared pathways, including secondary-metabolite biosynthesis (Fig. 5F). This points to a common feature: across habitats, the rhizosphere communities converge on functions related to interaction with host metabolites. In summary, the metagenomic data characterize the composition and host association of the *Rhododendron* rhizosphere community and reveal differences in its functional potential among species. The *R. bailiense* rhizosphere was enriched in functions related to phosphorus acquisition, nutrient cycling, aromatic-compound degradation and ion homeostasis. This functional profile suggests that microbial capacities may complement the host's genomic repertoire in the karst habitat.

Rhizosphere metagenomic functions covary with contrasting soil nutrient contexts

To determine whether the taxonomic differentiation described above was accompanied by functional differentiation, we compared KEGG level-3 pathways and nutrient-cycling genes across the rhizosphere metagenomes (Fig. 6A–F; Additional file 6). The three profiles were clearly distinct. The *R. bailiense* rhizosphere had higher abundances of bacterial chemotaxis, flagellar assembly, phosphonate and phosphinate metabolism, and pathways for the degradation of flavonoids, benzoate and limonene. The *R. delavayi* rhizosphere showed higher abundances of the nitrogen-cycle pathway, ABC transporters, carbon-fixation pathways and several amino-acid metabolic pathways, whereas the *R. ambiguum* rhizosphere had the highest abundance of the *Pseudomonas aeruginosa* biofilm-formation pathway. These differences indicate contrasting microbial functional repertoires among habitats rather than a simple gradient in overall metabolic activity.

Carbohydrate-active functions further distinguished the three rhizosphere communities (Fig. 6B). The *R. bailiense* metagenome contained the highest abundances of glucoamylase, arabinofuranosidase, β-mannanase, xylanase, endoglucanase, endo- and exochitinase, and pectinase genes, indicating broad potential to process starch, hemicellulose, cellulose, chitin and pectin. *R. delavayi* was comparatively enriched in xylose isomerase, acetylglucosaminidase, malate synthase, pyruvate-oxidation and acetogenesis functions, whereas *R. ambiguum* showed the highest abundances of α-amylase, pullulanase, isopullulanase, exoglucanase and acetate kinase. Thus, the three communities differed in their potential use of complex carbon substrates and fermentation products, providing a targeted basis for future substrate-use and process-rate measurements.

The soil measurements provide context for the phosphorus and nitrogen profiles. Both the *R. bailiense* and *R. delavayi* habitats had low total and available P (Fig. 1F, H). In the *R. delavayi* rhizosphere, *gcd*, *phoA*, *phoD* and phosphate-uptake genes (*pstS*, *pstA*, *pstB* and *pstC*) were generally most abundant among the three groups (Fig. 6C). By contrast, *R. bailiense* showed higher abundances of *ppa* and the C-P lyase-associated genes *phnM*, *phnI* and *phnJ*, consistent with its enrichment of the phosphonate and phosphinate metabolism pathway (Fig. 6A, C). Most of these P-acquisition genes were less abundant in the relatively P-rich *R. ambiguum* habitat. *R. delavayi* also showed the broadest enrichment across the nitrogen-cycle network, including genes involved in ammonia oxidation, assimilatory nitrate reduction, dissimilatory nitrate/nitrite reduction and organic-N assimilation (Fig. 6D). This functional profile is consistent with microbial transformation and recycling of limited nutrient pools in a habitat that had the lowest soil organic matter, total N and alkali-hydrolyzable N.

Sulfur-cycling genes showed pathway-specific, rather than uniformly higher, representation in any one habitat (Fig. 6E). The *R. delavayi* rhizosphere, despite having the lowest available S, had relatively high abundances of *sat*, *cysC*, *cysH*, *ttrA*, *sir* and *fccA*/*fccB*, whereas *R. bailiense* had higher abundances of *cysJ*, *soxC*, *soxY* and *sreB*. The *R. ambiguum* soil had the highest available S but did not show uniform dominance across these sulfur-transformation genes. Among functions related to environmental sensing and ion acquisition, *R. bailiense* had the highest abundances of the chemotaxis genes *cheA* and *cheY*, the manganese transporter *mntH* and the ferric-siderophore receptor *fhuA* (Fig. 6F). Although *mntH* primarily transports Mn^{2+} and Fe^{2+}, its enrichment in the high-Ca^{2+} *R. bailiense* habitat, together with *fhuA* and

chemotaxis genes, points to broader ion-homeostasis and micronutrient-acquisition adjustments that merit targeted physiological and transcriptomic study.

Together, these functional profiles covaried with the edaphic gradient (Figs. 1D–K, 6). The *R. bailiense* habitat combined high soil organic matter, total N and exchangeable Ca^{2+} with low P; the *R. delavayi* habitat was P-poor and had the lowest soil organic matter, total N, alkali-hydrolyzable N and available S; and the *R. ambiguum* habitat was relatively rich in P, alkali-hydrolyzable N and available S, with a pH of approximately 5. Exchangeable Ca^{2+} was lower in the *R. delavayi* and *R. ambiguum* habitats than in the *R. bailiense* habitat but remained at moderate levels. These associations suggest that each habitat supports a distinct microbial functional repertoire aligned with its resource profile. In *R. bailiense*, the combined enrichment of P-acquisition, complex-carbon-degradation and ion-homeostasis functions provides a plausible microbial complement to persistence in thin, P-poor, high-Ca^{2+} karst humus soil. Because host identity, habitat and geography covary in the present sampling, reciprocal-soil, transcriptomic and process-rate experiments will be especially valuable for testing this model.

Divergence of secondary metabolic profiles and identification of species-specific modules

To explore host secondary metabolites that may be associated with rhizosphere microbial differentiation, we characterized the leaf metabolomes of four *Rhododendron* species (Rb, Rd, Ram, Rde; Additional file 7; Additional file 3: Table S11). As detailed in the Methods (see "Non-targeted metabolomics analysis of leaves"), the leaf metabolome is used here as a practical proxy for species-specific host chemistry; metabolite–microbe links are therefore treated as candidate associations to be confirmed by future root and rhizosphere metabolomics. Among the annotated compounds, secondary metabolites dominated, with a substantial fraction of primary metabolites including lipids and carbohydrates (Additional file 1: Fig. S10A, B). Notably, *R. bailiense* and *R. ambiguum* possessed 311 and 838 unique metabolites, respectively, indicating pronounced interspecific divergence in metabolite composition (Additional file 1: Fig. S10C).

Principal component analysis of metabolite abundance revealed clear differentiation among *Rhododendron* species (Fig. 7A; R = 1, P = 0.001). *R. ambiguum*, *R. bailiense* and the *R. decorum*/*R. delavayi* pair occupied distinct regions of metabolic space. The close clustering of *R. delavayi* and *R. decorum* is consistent with contributions from their shared mixed-forest habitat and conserved host chemistry. Flavonoids (30.36%) and terpenoids (30.08%) were the two dominant classes in the *Rhododendron* secondary-metabolite repertoire (Fig. 7B).

Through WGCNA, we reduced the complex metabolic data into several highly correlated co-expression modules (Fig. 7C, D). *R. bailiense* exhibits a strong specificity dependence on the MEblue + MEcyan + MEgreenyellow modules, which are enriched with the dominant characteristic metabolites of *R. bailiense*. *R. ambiguum*'s dominant metabolic modules are identified as MEturquoise + MEpink + MEblack. *R. delavayi* shows the strongest positive correlation with the MEred module.

KEGG topology analysis further characterized the plant-group-associated modules (Fig. 7E, F). The *R. bailiense*-associated modules (MEblue + MEcyan + MEgreenyellow) were enriched in phenylpropanoid biosynthesis, alpha-linolenic-acid metabolism, and pantothenate and coenzyme-A biosynthesis. Phenylpropanoids are precursors of lignin and defensive flavonoids, while alpha-linolenic acid contributes to jasmonate-related stress signalling. These features suggest a coordinated chemical-defence and stress-signalling profile and prioritize phenylpropanoid and lipid-signalling metabolites for root and exudate assays. The *R. ambiguum*-associated modules (MEturquoise + MEpink + MEblack) were enriched in flavonoid and isoflavonoid biosynthesis, highlighting additional chemical candidates for rhizosphere interaction. Additional module-level pathway patterns are shown in Additional file 1: Figs. S11 and S12, and Additional file 7.

These results demonstrate species-specific divergence in leaf secondary-metabolite profiles across *Rhododendron*. *R. bailiense* was enriched in phenylpropanoid- and fatty-acid-related metabolites that may be relevant to chemical interactions in its karst habitat. These patterns provide candidates for future tests of metabolite-microbe associations.

Candidate associations between host metabolites and rhizosphere microbes

To identify key microorganisms and explore potential links between metabolites in the three focal *Rhododendron* species and their habitat-associated rhizosphere communities, we integrated metagenomic and metabolomic data and screened for covarying metabolite–taxon pairs. Among the top 30 metabolites ranked by variable importance in projection (VIP) across four *Rhododendron* species (Additional file 1: Fig. S13A), 3-hydroxyflavone and phosphoribosylformyl-glycinamidine were abundant in *R. delavayi*, whereas safynol and capillarisin were co-enriched in *R. bailiense* and *R. delavayi*. Safynol, a polyacetylene with reported broad-spectrum antimicrobial activity, is a candidate modulator of rhizosphere assembly. Metabolites in the modules most strongly correlated with each species showed high module membership and metabolite significance (Additional file 1: Fig. S13B–D).

A cross-domain co-occurrence network revealed a "core–periphery" topology linking metabolites and microbial genera (Fig. 8; Additional file 8). *Pseudorhodoplanes*, *Streptomyces* and *Candidatus Angelobacter* occupied central positions, positively correlated with many host

metabolites. This structure indicates that interspecific differences in host secondary metabolites (e.g. flavonoids, polyphenols, lipids) co-vary with the abundance of particular taxa rather than with single compounds. Several of these hub genera have functional attributes reported elsewhere that are potentially relevant on karst, including biocontrol and rhizosphere defence in *Streptomyces* and oligotrophic, recalcitrant-carbon and nitrogen cycling in *Candidatus Angelobacter* and *Pseudorhodoplanes*. These attributes are consistent with community-level functional potential relevant to nutrient turnover and stress-associated processes in karst soils.

We next examined the dominant species-specific metabolites and their associations with microbial taxa. The core metabolites of *R. bailiense* included luteolinidin, artonin K and 5,8,12-trihydroxy-9-octadecenoic acid (Additional file 1: Fig. S14A; Table 1; Additional file 3: Table S12); luteolinidin is a flavonoid signal reported to promote *Bacillus* chemotaxis toward roots, and artonin K has documented antimicrobial activity. The core metabolites of *R. ambiguum* included 4',7-dihydroxy-2',5-dimethoxyisoflavanone, curcumin I and umbelliprenin (Additional file 1: Fig. S14B; Table 1; Additional file 3: Table S12), and those of *R. delavayi* included heptadecatrienal and liquiritigenin (Additional file 1: Fig. S14C). These metabolites showed pronounced accumulation in their respective host species (Additional file 1: Fig. S14; Additional file 3: Table S12). Such species-specific chemistry provides candidate molecular correlates of microbial differentiation. In particular, the co-occurrence of *R. bailiense* metabolites with taxa carrying mineral-weathering or stress-related functions suggests specific chemical-filtering and resource-use hypotheses for direct testing.

Table 1

Representative metabolites and their reported or inferred microbial relevance in Rhododendron.

Species (Dominant module)	Key Metabolite Types	Dominant Metabolite	Rb	Ram	Rd	Rde	Representative microorganism
R. bailiense (MEblue)	Flavonoids and polyphenols	Luteolinidin	6.035 *	3.718	3.808	3.811	*Bacillus* (positive) / *Streptomyces* (positive)
		Artonin K	6.79 *	2.771	2.846	2.848	*Staphylococcus* (negative) / Pathogenic taxa (negative)
		3-Hydroxyphloretin 2'-O-glucoside	6.048 *	4.324	5.118	4.058	*Pseudorhodoplanes* (positive)
		Phloretin-2'-O-(2"-O-xylosylglucoside)	5.786 *	3.905	4.035	4.037	*Streptomyces* (positive)
		Ellagic acid acetyl-arabinoside	4.144 *	3.869	4.001	6.124 *	*Candidatus Angelobacter* (positive)
	Terpenes and saponins	Crinitol(Diterpenes)	6.196 *	3.324	3.588	3.46	*Streptomyces* (positive)
		7,13-Eperudien-15-oic acid(Diterpenes)	5.298 *	3.234	3.411	3.436	*Pseudorhodoplanes* (positive)
		Soyasapogenol D(Saponin aglycone)	6.876 *	1.454	1.582	1.651	*Candidatus Angelobacter* (positive)
		Pomolic acid(Triterpenes)	7.351 *	2.758	3.03	2.961	*Streptomyces* (positive)
	Oxidized lipids	8(s)-hetre	6.248 *	3.787	3.916	3.919	*Pseudorhodoplanes* (positive)
		PC(PGF1alpha/20:5(5Z,8Z,11Z,14Z,17Z))	6.921 *	1.453	1.675	1.65	*Candidatus Angelobacter* (positive)
	Quinone compounds	5,8-Dihydroxy-1,4-naphthoquinone	4.918 *	3.003	2.992	3.063	Pathogenic taxa (negative)
R. ambiguum (MEturquoise)	Isoflavones and flavonoids	4',7-Dihydroxy-2',5-dimethoxyisoflavanone	4.283	7.163 *	4.141	4.211	*Streptomyces* (positive)
		Sophoraflavanone b	0.7905	5.666 *	0.6663	0.668	*Pseudorhodoplanes* (positive)
		Licoricone	3.231	5.98 *	3.078	3.08	*Streptomyces* (positive)
		Betavulgarin xyloside	2.961	6.35 *	2.819	2.89	*Candidatus Angelobacter* (positive)
	Polyynes and coumarins	Falcarindione	0.9161	6.096 *	0.7941	0.8537	Redundant Saprotrophs (negative)
		Umbelliprenin	4.937	7.912 *	4.784	4.786	*Streptomyces* (positive)
	Curcumin and phenolic acids	Curcumin I	2.958	6.421 *	2.805	2.808	Pathogenic taxa (negative)
		Demethoxycurcumin	3.564	7.343 *	3.411	3.413	Pathogenic taxa (negative)

*Indicates metabolites significantly increased in the corresponding species ($P < 0.05$).

Species (Dominant module)	Key Metabolite Types	Dominant Metabolite	Rb	Ram	Rd	Rde	Representative microorganism
		Caffeic acid 3-glucoside	3.44	6.202 *	3.298	3.369	*Pseudorhodoplanes* (positive)
R. delavayi (MEred & MEtan)	Volatile compounds and terpenes	Heptadecatrienal	4.072	3.79	5.41 *	3.922	*Mehceanibacter* (positive)
		Piperdial	3.469	3.157	5.811 *	3.359	*Luteitalea* (positive)
		Furanogermenone	3.232	2.957	6.073 *	3.16	*Bradyrhizobium* (positive)
		5-Hydroxy-p-mentha-6,8-dien-2-one	3.254	2.927	6.464 *	3.13	*Streptomyces* (positive)
		Aromatic aldehyde	5.232	4.9	7.315 *	5.133	*Candidatus Angelobacter* (positive)
	Oxidized lipids and hormone-related metabolites	14,15-DiHETrE	3.685	3.411	5.979 *	3.614	*Pseudorhodoplanes* (positive)
		Abscisic alcohol 11-glucoside	3.108	2.644	6.143 *	2.847	*Streptomyces* (positive)
	Plant defense compounds and alkaloids	Chalcomoracin	4.306	4.023	7.074 *	4.303	Pathogenic taxa (negative)
		Annoglabasin B	3.138	2.864	5.066 *	3.066	*Candidatus Angelobacter* (positive)
		Liensinine	4.3	3.974	7.327 *	4.177	*Streptomyces* (positive)
	Glycyrrhizin and cinnamic acid	Liquiritigenin	3.611	3.299	5.961 *	3.583	*Mehceanibacter* (positive)
		2-Hydroxycinnamic acid	5.115	4.868	6.503 *	5.069	*Pseudorhodoplanes* (positive)

*Indicates metabolites significantly increased in the corresponding species ($P < 0.05$).

Integrating the multi-omics evidence (Figs. 1–8; Additional file 1: Figs. S13–S14; Table 1), a consistent picture emerges in which *Rhododendron* lineages with distinct genomic features accumulate species-specific secondary-metabolite profiles that co-vary with the composition and functional potential of their rhizosphere communities. This coordinated pattern supports a working model in which host chemistry helps shape functionally biased microbial assemblages whose capacities may complement host genomic traits under environmental stress, and it defines tractable candidates for testing functional team assembly in *Rhododendron*.

Discussion

By integrating comparative genomics, non-targeted leaf metabolomics, fungal ITS profiling and deep metagenomic sequencing, this study resolves coordinated differentiation across host genomes, leaf chemistry and rhizosphere communities in contrasting *Rhododendron* habitats. This cross-kingdom design is a central strength: the karst-endemic *R. bailiense* differs from widespread comparators across all three biological layers, and the alignment of these patterns points to a linked ecological strategy for persistence in high-Ca^{2+}, drought-prone and P-poor karst substrates [6, 9].

From specialist rock-weathering to generalist saprotrophy: habitat-associated fungal niche differentiation as a candidate extended phenotype

When discussing the environmental adaptability of plants, the traditional Modern Synthesis primarily focuses on the changes in allele frequencies of the host itself [36]. Our results can be considered within the holobiont framework, which treats host-associated microorganisms as potential contributors to plant phenotype and ecological performance [37].

The Functional Team Selection (FTS) framework provides a useful hypothesis-generating context for interpreting these associations [5]. Within this framework, host traits and environmental conditions may jointly favour microbial assemblages with particular functional capacities under resource limitation or abiotic stress [5, 38]. Root-secreted secondary metabolites may act as chemical cues or ecological filters, and the present co-variation patterns nominate specific compounds and taxa for direct tests of microbial assembly and functional complementarity [5, 15].

The differences in prokaryotic and eukaryotic alpha and beta diversity among the three *Rhododendron* rhizospheres are consistent with habitat- and host-associated community assembly. The widespread *R. delavayi*, growing in deeper but comparatively nutrient-poor and P-poor yellow soil, hosted a more diverse rhizosphere community with prominent saprotrophic and nutrient-turnover potential. In contrast, the endemic *R. bailiense*, in high-Ca^{2+}, phosphorus-poor humus within karst rock crevices, harboured a markedly less diverse community dominated by a few taxa, notably *Piloderma* and *Bradyrhizobium*. This contrast in community diversity and dominant taxa parallels the classic association between Ericaceae and specialized mycorrhizal fungi, which help these plants acquire nutrients on acidic, nutrient-poor substrates [39]. The genomic features of *R. bailiense* are consistent with such a host–microbe association [5] (Additional file 2: Note S5).

Under the extended-phenotype framework, the functional genes carried by the rhizosphere community can be viewed as a spatial extension of the host's own functional repertoire [40, 41]. The fungal communities illustrate this most clearly: we observed a phylum/genus-level turnover among the three species, with the *R. bailiense* rhizosphere dominated by the basidiomycete *Piloderma* and those of *R. delavayi* and *R. ambiguum* enriched in *Ascomycota* and *Mortierellomycota*. *Piloderma*, an ectomycorrhizal, mineral-weathering basidiomycete, is well documented as a biological weathering agent that mobilizes phosphorus and chelates calcium [42, 43] (Additional file 2: Note S6); its dominance in the *R. bailiense* rhizosphere is therefore of particular interest on phosphorus-limited karst, although whether it forms a functional mycorrhiza with *R. bailiense* remains to be confirmed. By contrast, the *R. delavayi* and *R. ambiguum* rhizospheres were enriched in *Mortierella*, a widespread generalist saprotroph and recognized plant-growth-promoting fungus [44–46] (Additional file 2: Note S6), consistent with the broader habitats of these two widely distributed species.

Host-associated functional potential of the prokaryotic rhizosphere community

Alongside the differentiation of fungal communities, the prokaryotic fraction of the rhizosphere may contribute to host functional adaptation [40]. KEGG-based comparison of the metagenomes showed that the three *Rhododendron* rhizospheres differed not only in taxonomic composition but also in the functional potential of pathways related to carbon, nitrogen and sulfur cycling. The soil measurements place these functional-potential patterns within quantified edaphic gradients; however, the design does not separate host identity from habitat and geography, and the identity and reported functions of the taxa enriched in the *R. bailiense* rhizosphere offer useful early insight into which microbial groups may be relevant to *Rhododendron* adaptation on karst.

Three groups are of particular interest. First, genes for bacterial chemotaxis and flagellar assembly (e.g. *cheA*, *cheY*) were enriched in the *R. bailiense* rhizosphere. Given that karst bare-rock habitats are highly heterogeneous, with moisture and nutrients confined to transient, patchy microsites [6, 7], enrichment of motility- and sensing-related functions suggests a community with the potential to track resource gradients and colonize the root surface efficiently [3, 47].

Second, *Bradyrhizobium* was a dominant member of the non-leguminous *R. bailiense* rhizosphere (Additional file 2: Note S7). The absence of detectable *nifH* in the *R. bailiense* metagenomes, together with the high total-N content of its humus soil, suggests that the prominence of this genus may reflect functions other than, or in addition to, nitrogen fixation. Oligotrophic persistence, organic-substrate use and interaction with Ericaceae roots are priority hypotheses for strain-resolved genomics and physiological testing.

Third, the *R. bailiense* rhizosphere was enriched in the uncultured acidobacterial genus *Candidatus Sulfotelmatobacter*, whose characterized representatives possess dissimilatory sulfur-metabolism potential [48]. Consistent with a broader community-level shift in sulfur metabolism, *cysJ*, *soxC*, *soxY* and *sreB* were more abundant in the *R. bailiense* group than in the other two groups. Because microbial sulfur oxidation can generate protons, this functional profile could, in principle, influence local mineral weathering and microscale pH, with downstream effects on the availability of trace elements such as iron. This possibility is especially relevant given the concurrent enrichment of the *fhuA* iron-transporter receptor.

Together, these observations characterize the prokaryotic rhizosphere of karst *Rhododendron* and nominate *Bradyrhizobium*, sulfur-cycling bacteria and highly motile, chemotactic groups as candidate contributors to nutrient turnover, stress tolerance and root-zone persistence. Finer-scale rhizosphere-chemistry measurements, isolation of key strains and manipulative inoculation experiments can now test how these groups affect host performance.

Species-specific leaf chemistry and candidate associations with the rhizosphere community

The four *Rhododendron* species differed markedly in their leaf secondary-metabolite profiles, with safynol, luteolinidin and artonin K prominent in *R. bailiense*-associated chemistry (Additional file 2: Note S8). Polyacetylenes can constrain sensitive microbes, whereas flavonoids can serve as microbial substrates or chemotactic cues. Consistent with these functions, luteolinidin, phloretin glycosides and several diterpenoid features were linked in the candidate map to *Bacillus*, *Streptomyces* or *Pseudorhodoplanes* (Table 1; Additional file 8; Additional file 2: Notes S8, S9), providing concrete hypotheses for metabolite-guided assembly. In *R. ambiguum*, isoflavonoids, umbelliprenin and curcumin-related features were paired with *Streptomyces* or *Pseudorhodoplanes*, whereas furanogermenone and liquiritigenin in *R. delavayi* were paired with *Bradyrhizobium* or *Mehceanibacter*. These patterns suggest niche partitioning through substrate preference, chemotaxis, metabolite transformation and selective antimicrobial effects.

Plant secondary metabolites or their precursors can move systemically to roots, where local conversion and exudation may expose rhizosphere microbes to host-derived chemistry [49–51] (Additional file 2: Note S8). The leaf profiles therefore provide a practical inventory of compounds that could enter belowground pathways. Our data establish their presence at the species level, while direct enrichment in roots remains a focused question for future work. We are refining low-biomass root collection, cleaning and microextraction procedures to determine which metabolites accumulate in roots and how they relate to recruited microbial consortia.

A multi-omics correlation network showed non-random core–periphery structure and identified *Streptomyces*, *Pseudorhodoplanes* and *Candidatus Angelobacter* as candidate key microorganisms (Fig. 8; Additional file 8; Additional file 2: Note S9). Their reported or predicted capacities for specialized-metabolite transformation, biosynthetic diversity and recalcitrant-carbon processing suggest routes by which host chemical repertoires could be matched to microbial resource use and defence. Together, the network prioritizes specific compound–taxon pairs for root-exudate assays, strain-level genomics and inoculation experiments.

The cross-species contrasts extend this model beyond the best-known compounds. Artonin K, phloretin glycosides and terpene features in *R. bailiense*, curcumin-related compounds and umbelliprenin in *R. ambiguum*, and phenylpropanoid, flavonoid and terpene features in *R. delavayi* define additional candidate links to *Streptomyces*, *Pseudorhodoplanes*, *Bradyrhizobium* and other key taxa (Table 1; Additional file 8; Additional file 2: Notes S8, S9). Each host chemical repertoire may therefore provide a distinct combination of substrates, signals and selective pressures that aligns with microbial resource use, chemical tolerance or biotransformation.

Conclusions

Overall, multi-omics reveal coordinated genomic, chemical and rhizosphere differentiation across *Rhododendron* habitats, with complementary host and microbial traits in *R. bailiense*. Reciprocal-soil, root/exudate and strain-resolved experiments should test habitat filtering, host enrichment and functional exchange.

Abbreviations

ACE	Abundance-based coverage estimator
ASV	Amplicon sequence variant
BRNR	Baili Rhododendron Nature Reserve
DDA	Data-dependent acquisition
DMs	Differential metabolites
ESI	Electrospray ionization
FTS	Functional Team Selection
GO	Gene Ontology
ITS	Internal transcribed spacer
KEGG	Kyoto Encyclopedia of Genes and Genomes
LDA	Linear discriminant analysis
LEfSe	Linear discriminant analysis effect size

NR	Non-redundant protein sequence database
ORF	Open reading frame
PCA	Principal component analysis
PCoA	Principal coordinates analysis
PLS-DA	Partial least squares discriminant analysis

Ram *Rhododendron ambiguum*

Rb *Rhododendron bailiense*

Rd *Rhododendron delavayi*

Rde *Rhododendron decorum*

TPM	Transcripts per million
UHPLC-MS/MS	Ultra-high-performance liquid chromatography–tandem mass spectrometry
VIP	Variable importance in projection
WGCNA	Weighted gene co-expression network analysis

Declarations

Ethics approval and consent to participate

Not applicable (this study did not involve human participants or animals). Collection of plant and soil samples was carried out with permission from [the Administration of the Baili Rhododendron Nature Reserve and the relevant authority for Wawu Mountain]. The collection of plant material complied with relevant institutional, national and international guidelines and legislation, and followed the IUCN Policy Statement on Research Involving Species at Risk of Extinction and the Convention on the Trade in Endangered Species of Wild Fauna and Flora.

Consent for publication

Not applicable.

Availability of data and materials

The raw metagenomic and fungal ITS sequencing data are available at China National Center for Bioinformation (https://ngdc.cncb.ac.cn/gsa/), with GSA access number CRA042167 (Bioproject: PRJCA063219). The metabolomics data were deposited in the MetaboLights database (https://www.ebi.ac.uk/metabolights/) under the project number MTBLS14427. Additionally, the annotation and abundance data derived from the metagenomic, fungal ITS, and metabolomic analyses are provided in Additional files 4–8.

Competing interests

The authors declare no competing interests.

Funding

This study was supported by grants from the National Natural Science Foundation of China (32602618; 32560390), General program of China Postdoctoral Science Foundation (2026M792796); Guizhou Provincial Basic Research Program (Natural Science) (Qiankehe Foundation MS[2026]093), Major Scientific and Technological Project of the Guizhou Provincial Forestry Department (Qian Lin Ke He [2026] Key Project No. 002), as well as Open Research Fund Program of Guizhou Key Laboratory of Forest Cultivation in Plateau Mountain (LMPY202511).

Authors' contributions

SLW and GJD conceived and supervised the project. GJD and SLW designed the experiments. SLW, YXL, HLY, KZ, YM, and LP performed the experiments. SLW analyzed the data and wrote the article. GQ and GJD revised the manuscript. JO, GQ, XPW, and GJD provided research suggestions and assisted in reviewing the manuscript. SLW and GJD acquired the funding. All authors read and approved the final manuscript.

References

1. Vandenkoornhuyse P, Quaiser A, Duhamel M, Le Van A, Dufresne A. The importance of the microbiome of the plant holobiont. New Phytol. 2015;206:1196–206.
2. Manzanera M. From microbial consortia to ecosystem resilience: the integrative roles of holobionts in stress biology. Biology (Basel). 2025;14:1203.
3. Zhalnina K, Louie KB, Hao Z, Mansoori N, da Rocha UN, Shi S, et al. Dynamic root exudate chemistry and microbial substrate preferences drive patterns in rhizosphere microbial community assembly. Nat Microbiol. 2018;3:470–80.
4. Fromm E, Zinger L, Pellerin F, Di Gesu L, Jacob S, Winandy L, et al. Warming effects on lizard gut microbiome depend on habitat connectivity. Proc Biol Sci. 2024;291:20240220.
5. Johnson NC, Marin C. Functional team selection as a framework for local adaptation in plants and their belowground microbiomes. ISME J. 2025;19:wraf137.
6. Feng C, Wang J, Wu L, Kong H, Yang L, Feng C, et al. The genome of a cave plant, *Primulina huaijiensis*, provides insights into adaptation to limestone karst habitats. New Phytol. 2020;227:1249–63.
7. Liu C, Huang Y, Wu F, Liu W, Ning Y, Huang Z, et al. Plant adaptability in karst regions. J Plant Res. 2021;134:889–906.
8. Liu X, Ma Y. Genomic insights into the survival code of karst plants. Plant Divers. 2026.
9. Sardans J, Lambers H, Preece C, Alrefaei AF, Penuelas J. Role of mycorrhizas and root exudates in plant uptake of soil nutrients (calcium, iron, magnesium, and potassium): has the puzzle been completely solved? Plant J. 2023;114:1227–42.
10. Wen S, Zhou K, Min Y, Yang K, Shang C, Peng L, et al. The evolution of Ca^{2+}-ATPases across plants with profiles in rhododendron and the function of key members in alleviating high calcium stress. Hortic Res. 2026;uhag174. https://doi.org/10.1093/hr/uhag174.
11. Wen S, Cai X, Zhou K, Min Y, Shang C, Shen L, et al. Metabolome and comparative genome provide insights into secondary metabolites generation of a rare karst-growing *Rhododendron* in vitro culture. Plant J. 2025;121:e17235.
12. Wen S, Cai X, Yang K, Hong Y, Fan F, Wang Q, et al. Chromosome-level genome assembly of a rare karst-growing *Rhododendron* species provides insights into its evolution and environmental adaptation. J Syst Evol. 2025;63:245–67.
13. Luo YH, Ma LL, Cadotte MW, Seibold S, Zou JY, Song J, et al. Ericoid mycorrhizal fungal metacommunity facilitates closely related *Rhododendron* species coexistence. New Phytol. 2025;248:1442–57.
14. Layeghifard M, Hwang DM, Guttman DS. Disentangling interactions in the microbiome: a network perspective. Trends Microbiol. 2017;25:217–28.
15. Yu P, He X, Baer M, Beirinckx S, Tian T, Moya YAT, et al. Plant flavones enrich rhizosphere Oxalobacteraceae to improve maize performance under nitrogen deprivation. Nat Plants. 2021;7:481–99.
16. Pang Z, Chen J, Wang T, Gao C, Li Z, Guo L, et al. Linking plant secondary metabolites and plant microbiomes: a review. Front Plant Sci. 2021;12:621276.
17. Greger H. Comparative phytochemistry of polyacetylenes of the genus *Artemisia* (Asteraceae): compounds with high biological activities and chemotaxonomic significance. Molecules. 2025;30:537.
18. Goel M, Sun H, Jiao WB, Schneeberger K. SyRI: finding genomic rearrangements and local sequence differences from whole-genome assemblies. Genome Biol. 2019;20:277.
19. Bolyen E, Rideout JR, Dillon MR, Bokulich NA, Abnet CC, Al-Ghalith GA, et al. Reproducible, interactive, scalable and extensible microbiome data science using QIIME 2. Nat Biotechnol. 2019;37:852–7.
20. Callahan BJ, McMurdie PJ, Rosen MJ, Han AW, Johnson AJ, Holmes SP. DADA2: high-resolution sample inference from Illumina amplicon data. Nat Methods. 2016;13:581–3.
21. Wang Q, Garrity GM, Tiedje JM, Cole JR. Naive Bayesian classifier for rapid assignment of rRNA sequences into the new bacterial taxonomy. Appl Environ Microbiol. 2007;73:5261–7.
22. Nilsson RH, Larsson KH, Taylor AFS, Bengtsson-Palme J, Jeppesen TS, Schigel D, et al. The UNITE database for molecular identification of fungi: handling dark taxa and parallel taxonomic classifications. Nucleic Acids Res. 2019;47:D259–64.

23. Chen S, Zhou Y, Chen Y, Gu J. fastp: an ultra-fast all-in-one FASTQ preprocessor. Bioinformatics. 2018;34:i884–90.
24. Li D, Liu CM, Luo R, Sadakane K, Lam TW. MEGAHIT: an ultra-fast single-node solution for large and complex metagenomics assembly via succinct de Bruijn graph. Bioinformatics. 2015;31:1674–6.
25. Hyatt D, Chen GL, Locascio PF, Land ML, Larimer FW, Hauser LJ. Prodigal: prokaryotic gene recognition and translation initiation site identification. BMC Bioinformatics. 2010;11:119.
26. Fu L, Niu B, Zhu Z, Wu S, Li W. CD-HIT: accelerated for clustering the next-generation sequencing data. Bioinformatics. 2012;28:3150–2.
27. Li R, Yu C, Li Y, Lam TW, Yiu SM, Kristiansen K, et al. SOAP2: an improved ultrafast tool for short read alignment. Bioinformatics. 2009;25:1966–7.
28. Buchfink B, Xie C, Huson DH. Fast and sensitive protein alignment using DIAMOND. Nat Methods. 2015;12:59–60.
29. Hou Y, Wei W, Guan X, Liu Y, Bian G, He D, et al. A diet-microbial metabolism feedforward loop modulates intestinal stem cell renewal in the stressed gut. Nat Commun. 2021;12:271.
30. Zhang H, Huang M, Zhang W, Gardea-Torresdey JL, White JC, Ji R, et al. Silver nanoparticles alter soil microbial community compositions and metabolite profiles in unplanted and cucumber-planted soils. Environ Sci Technol. 2020;54:3334–42.
31. Schloss PD, Westcott SL, Ryabin T, Hall JR, Hartmann M, Hollister EB, et al. Introducing mothur: open-source, platform-independent, community-supported software for describing and comparing microbial communities. Appl Environ Microbiol. 2009;75:7537–41.
32. Segata N, Izard J, Waldron L, Gevers D, Miropolsky L, Garrett WS, et al. Metagenomic biomarker discovery and explanation. Genome Biol. 2011;12:R60.
33. Douglas GM, Maffei VJ, Zaneveld JR, Yurgel SN, Brown JR, Taylor CM, et al. PICRUSt2 for prediction of metagenome functions. Nat Biotechnol. 2020;38:685–8.
34. Nguyen NH, Song Z, Bates ST, Branco S, Tedersoo L, Menke J, et al. FUNGuild: an open annotation tool for parsing fungal community datasets by ecological guild. Fungal Ecol. 2016;20:241–8.
35. Langfelder P, Horvath S. WGCNA: an R package for weighted correlation network analysis. BMC Bioinformatics. 2008;9:559.
36. Huitzil S, Huepe C, Aldana M, Frank A. The missing link: how the holobiont concept provides a genetic framework for rapid evolution and the inheritance of acquired characteristics. Front Ecol Evol. 2023;11:1279938.
37. Lyu DM, Zajonc J, Pagé A, Tanney CAS, Shah A, Monjezi N, et al. Plant holobiont theory: the phytomicrobiome plays a central role in evolution and success. Microorganisms. 2021;9:675.
38. Liu H, Brettell LE, Qiu Z, Singh BK. Microbiome-mediated stress resistance in plants. Trends Plant Sci. 2020;25:733–43.
39. Martino E, Morin E, Grelet GA, Kuo A, Kohler A, Daghino S, et al. Comparative genomics and transcriptomics depict ericoid mycorrhizal fungi as versatile saprotrophs and plant mutualists. New Phytol. 2018;217:1213–29.
40. Trivedi P, Leach JE, Tringe SG, Sa T, Singh BK. Plant–microbiome interactions: from community assembly to plant health. Nat Rev Microbiol. 2020;18:607–21.
41. Kural-Rendon C, Ford NE, Hooser K, Wagner MR. Intraspecific plant-soil feedbacks alter root traits in a perennial grass. Rhizosphere. 2025;35.
42. King K, Fransson P, Finlay R, Sanchez-Garcia M. Transporter gene family evolution in ectomycorrhizal fungi in relation to mineral weathering capabilities. Biogeosciences. 2025;22:8047–64.
43. Tuason MMS, Arocena JM. Calcium oxalate biomineralization by *Piloderma fallax* in response to various levels of calcium and phosphorus. Appl Environ Microbiol. 2009;75:7079–85.
44. Vandepol N, Liber J, Desirò A, Na H, Kennedy M, Barry K, et al. Resolving the Mortierellaceae phylogeny through synthesis of multi-gene phylogenetics and phylogenomics. Fungal Divers. 2020;104:267–89.
45. Ozimek E, Hanaka A. *Mortierella* species as the plant growth-promoting fungi present in the agricultural soils. Agric (Basel). 2021;11:7.
46. De Tender C, Vandecasteele M, Ommeslag S, De Zutter N, Vandenbussche E, Haegeman A, et al. *Linnemannia elongata*: a key species in chitin-based plant growth promotion. Phytobiomes J. 2024;8:366–77.
47. Bais HP, Weir TL, Perry LG, Gilroy S, Vivanco JM. The role of root exudates in rhizosphere interactions with plants and other organisms. Annu Rev Plant Biol. 2006;57:233–66.
48. Hausmann B, Pelikan C, Herbold CW, Köstlbacher S, Albertsen M, Eichorst SA, et al. Peatland Acidobacteria with a dissimilatory sulfur metabolism. ISME J. 2018;12:1729–42.
49. Buer CS, Muday GK, Djordjevic MA. Flavonoids are differentially taken up and transported long distances in *Arabidopsis*. Plant Physiol. 2007;145:478–90.

50. McLaughlin S, Zhalnina K, Kosina S, Northen TR, Sasse J. The core metabolome and root exudation dynamics of three phylogenetically distinct plant species. Nat Commun. 2023;14:1649.
51. Korenblum E, Dong Y, Szymanski J, Panda S, Jozwiak A, Massalha H, et al. Rhizosphere microbiome mediates systemic root metabolite exudation by root-to-root signaling. Proc Natl Acad Sci U S A. 2020;117:3874–83.

Figures

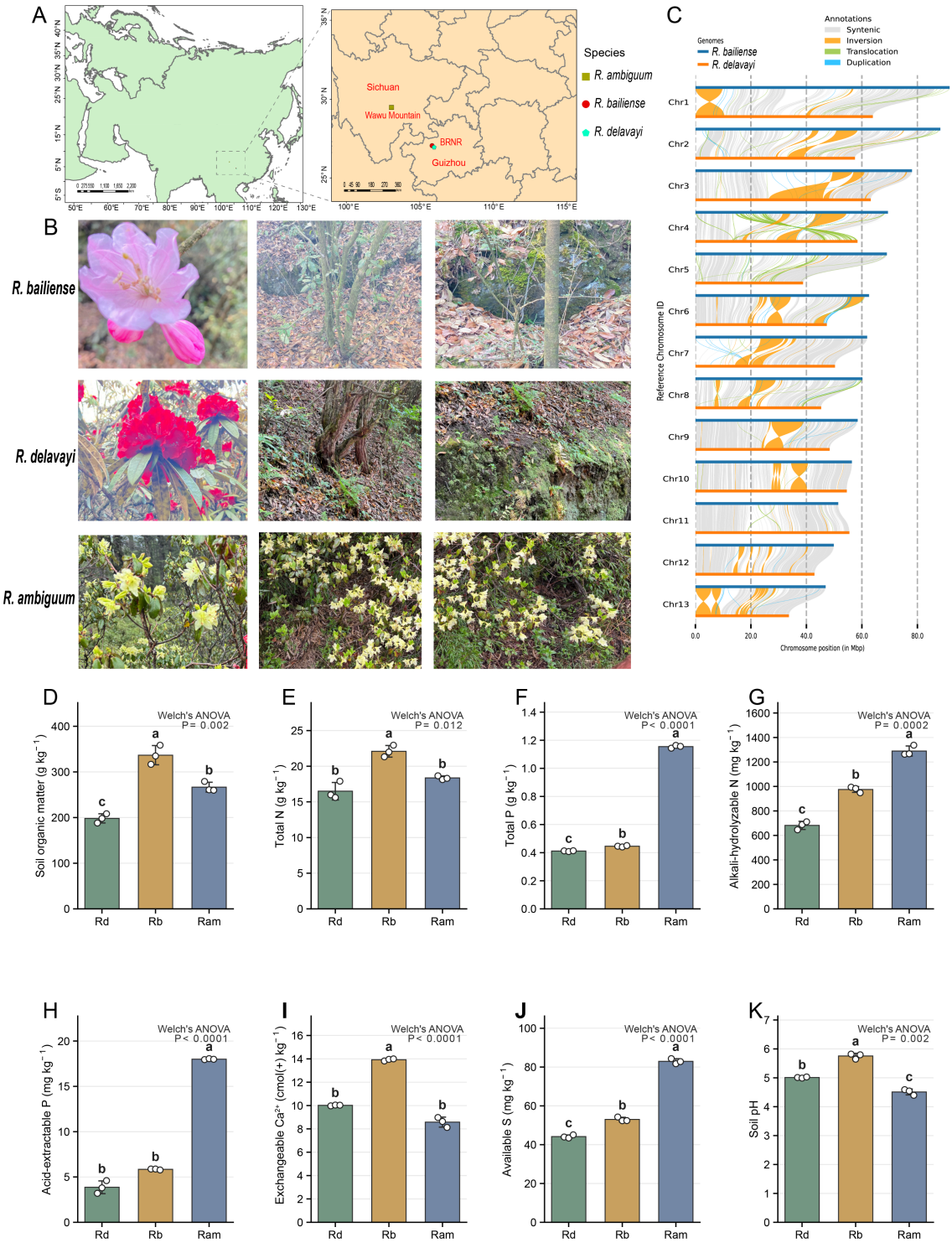


Figure 1

Habitat divergence, soil physicochemical properties and comparative genomic signatures of three typical *Rhododendron* species. (A) Locations of the Baili *Rhododendron* Nature Reserve (BRNR) in Guizhou and Wawu Mountain in Sichuan, where habitat soils were sampled. (B) Representative plant phenotypes and habitat conditions for *R. bailiense*, *R. delavayi* and *R. ambiguum*. *R. bailiense* occurs on exposed karst summits with shallow, discontinuous soil; *R. delavayi* occurs in mountain yellow soil; and *R. ambiguum* occurs in acidic yellow-brown soil. (C) Whole-genome structural comparison and synteny mapping between *R. bailiense* and *R. delavayi*. (D-K) Soil organic matter, total N, total P, alkali-hydrolyzable N, available P, exchangeable Ca^{2+}, available S and soil pH, respectively, in the habitats of *R. delavayi* (Rd), *R. bailiense* (Rb) and *R. ambiguum* (Ram). Bars show group means, with individual replicate measurements overlaid. P values are from Welch's ANOVA; different lowercase letters indicate significant differences among habitats.

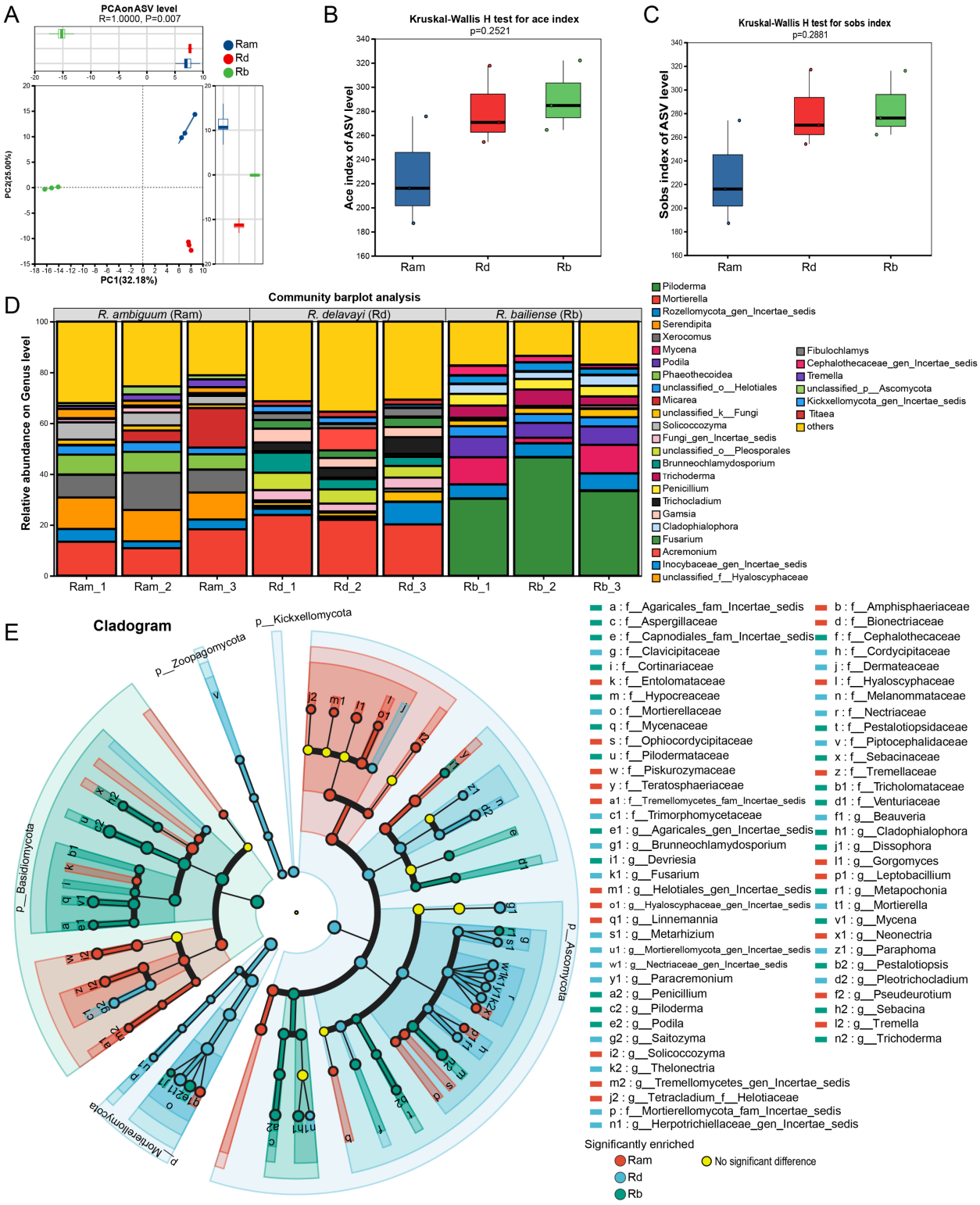


Figure 2

Fungal ITS (Internal Transcribed Spacer) sequencing of soils from three *Rhododendron* habitats. (A) PCoA (Principal Coordinates Analysis) reveals differences in fungal composition (ASV level) among the three soil types. (B & C) Comparison of two alpha diversity indices (ACE index and Sobs index) across the three samples. (D) Bar charts illustrate the differences in abundance and proportion of fungal genera across the nine soil samples (three types). (E) The LEfSe multi-level species hierarchy tree illustrates species differences among fungi at various taxonomic levels across the three soil sample categories. Nodes of different colors indicate fungal taxa that are significantly enriched within their respective groups and have a significant impact on intergroup differences; light yellow nodes indicate fungal taxa that show no significant differences across groups. From the interior to the exterior of the tree, the taxonomic levels progress from the phylum level to the genus level. For annotations, those beginning with “p__” indicate the phylum level; those beginning with “f__” indicate the family level; and those beginning with “g__” indicate the genus level. Abbreviations in the figure: Ram, *R. ambiguum*; Rb, *R. bailiense*; Rd, *R. delavayi*. For fungal annotations and abundance data, please refer to Additional file 4.

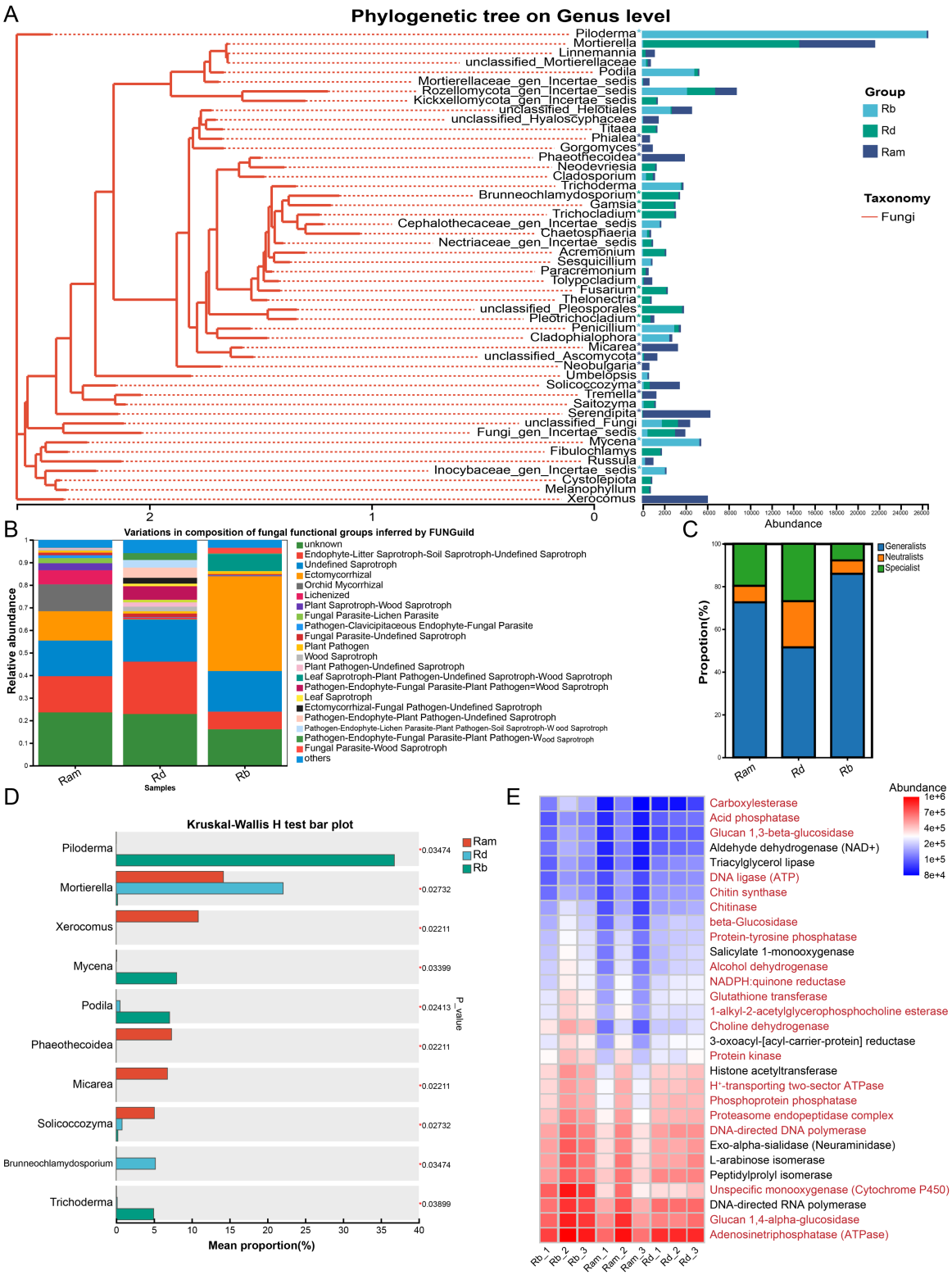


Figure 3

Fungal typological characteristics in the three soil sample categories. (A) The phylogenetic tree (genus level) reveals the phylogenetic relationships and evolutionary distances among the detected species, while the bar chart illustrates their relative abundances across different groups. The different colored asterisks indicate the dominant fungal genera found in the corresponding *Rhododendron* species selected through filtering; these fungal groups exhibit evolutionary clustering and specificity toward the associated *Rhododendron* species. (B) Differences in fungal functional group composition among the three soil sample categories, as predicted based on the FUNGuild database. (C) Proportions of generalist, specialist, and intermediate fungal groups in the three soil sample categories. This figure illustrates the degree of variability in fungal community ecotypes across different experimental groups during the succession stage. The classification of fungal types in this figure is derived from calculations based on the associated data in Additional file 1: Fig. S6A. (D) Bar charts display the

10 fungal genera with the most pronounced differences between groups. (E) The heatmap compares the abundance differences of the top 30 fungal-associated enzymes across the nine samples. This figure illustrates the distribution of major dominant functions across different samples. Red text indicates enzymes with significant changes in abundance ($P < 0.05$). Significance was tested using the Kruskal-Wallis H test (*, $P < 0.05$).

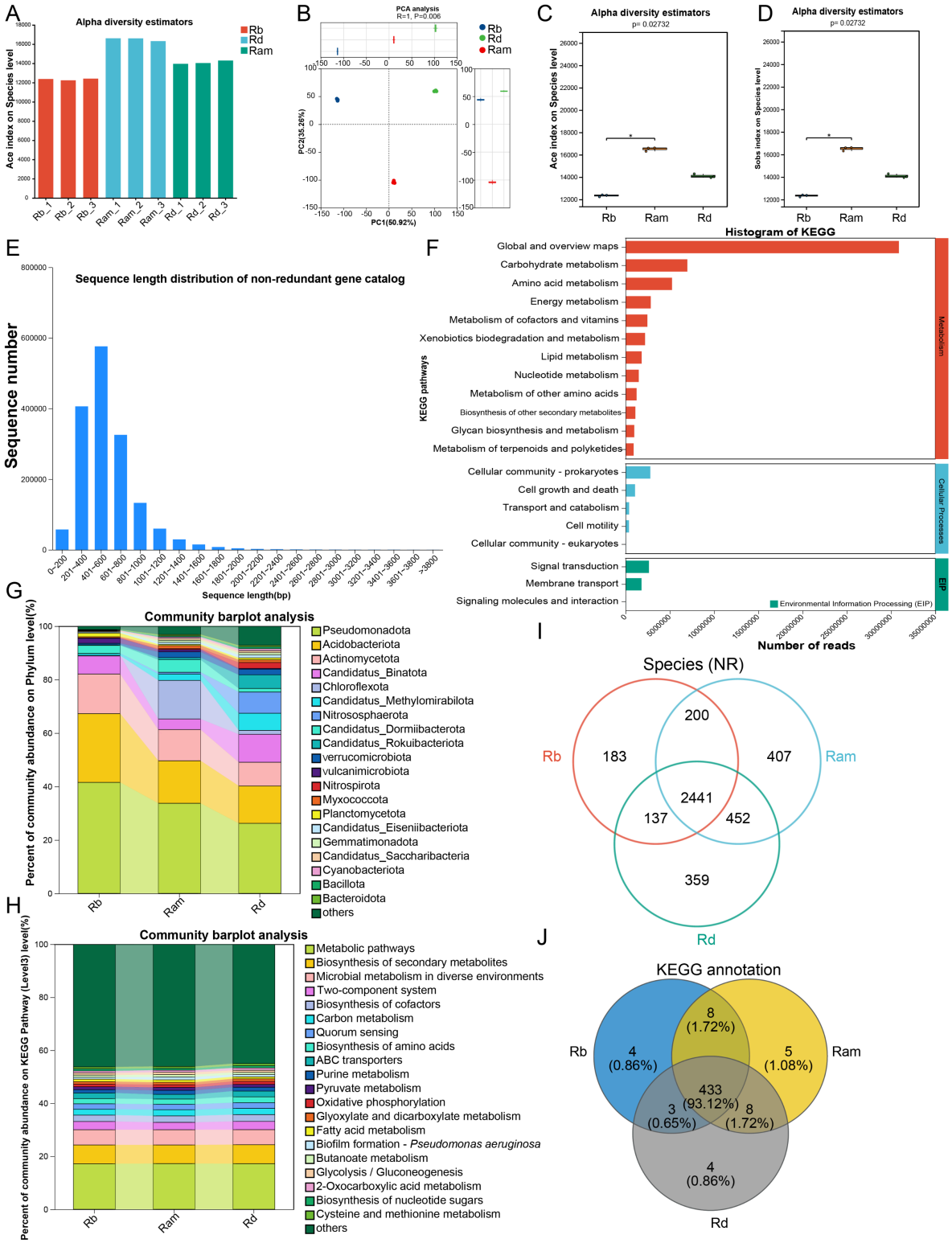


Figure 4

Metagenomic sequencing analysis of three soil sample types. (A) Comparison of the alpha diversity index (ACE index) across nine samples. (B) PCoA reveals differences in the microbial metagenomes among the three soil types. (C & D) Comparison of two alpha diversity indices (ACE index and Sobs index) for the metagenomes of the three sample types. (E) Sequence length distribution of the non-redundant gene

catalog obtained from metagenomic sequencing analysis. (F) Functional enrichment analysis of annotated gene sequences. (G) Bar charts showing the differences in abundance and proportion of microbial genera in the three soil sample categories based on metagenomic data. (H) A bar chart showing the differences in abundance and proportion of microbial KEGG-annotated functions across the three soil samples. (I) A Venn diagram showing the distribution of shared and unique microbial genera across the three soil types based on metagenomic analysis. (J) A Venn diagram showing the distribution of shared and unique KEGG annotations across the three soil types based on metagenomic analysis. For metagenomic annotation information, please refer to Additional file 5.

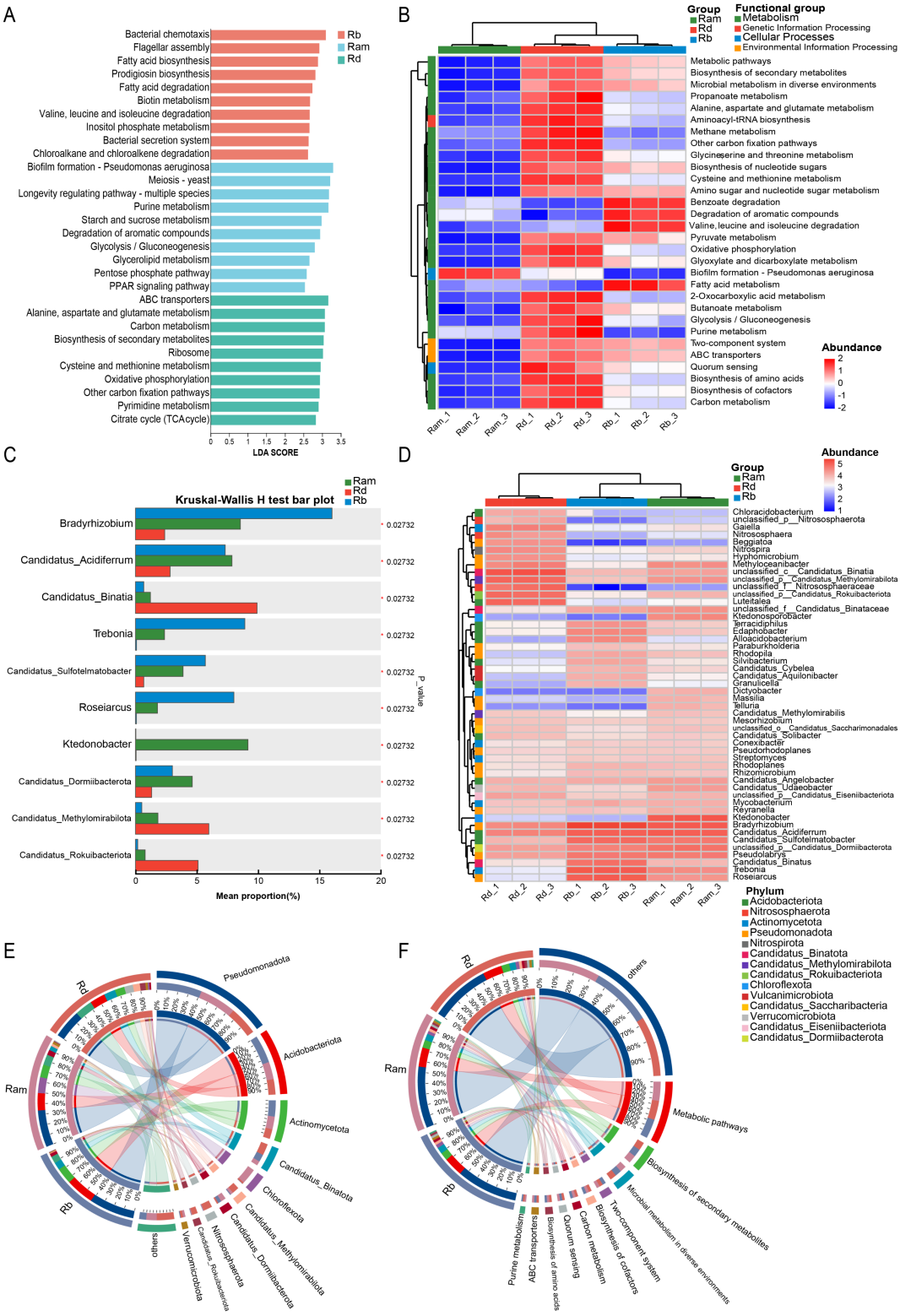


Figure 5

Differences in microbial composition among the three soil sample groups. (A) The bar chart displays the LDA (Linear Discriminant Analysis) values for different differential microbial functions across groups. This figure visually illustrates the magnitude of influence that differential microbial functions exert on the differences between groups, serving to identify significantly contributing microbial functions. A higher LDA value indicates that the corresponding function has a greater impact on the observed differences. (B) The heatmap displays a comparison of abundance differences for the top 30 pathways (Level 3, KEGG annotation) based on metagenomic analysis across the nine samples. Significant changes were observed in all pathways ($P < 0.05$). (C) The bar chart shows the 10 microbial genera (all bacteria) with the most pronounced differences between groups based on metagenomic analysis. (D) The heatmap displays the abundance differences of the top 50 microbial genera (based on metagenomic analysis) across the three soil types. All genera showed significant changes ($P < 0.05$). (E) The Circos plot illustrates the distribution of dominant species across the three soil sample types. (F) The Circos plot illustrates the distribution of major microbial functions across the three soil sample types. The left semicircle (smaller circle) represents the microbial species/functional abundance composition of the samples, while the right semicircle (larger circle) represents the distribution proportion of species/functions across different samples at that clustering level.

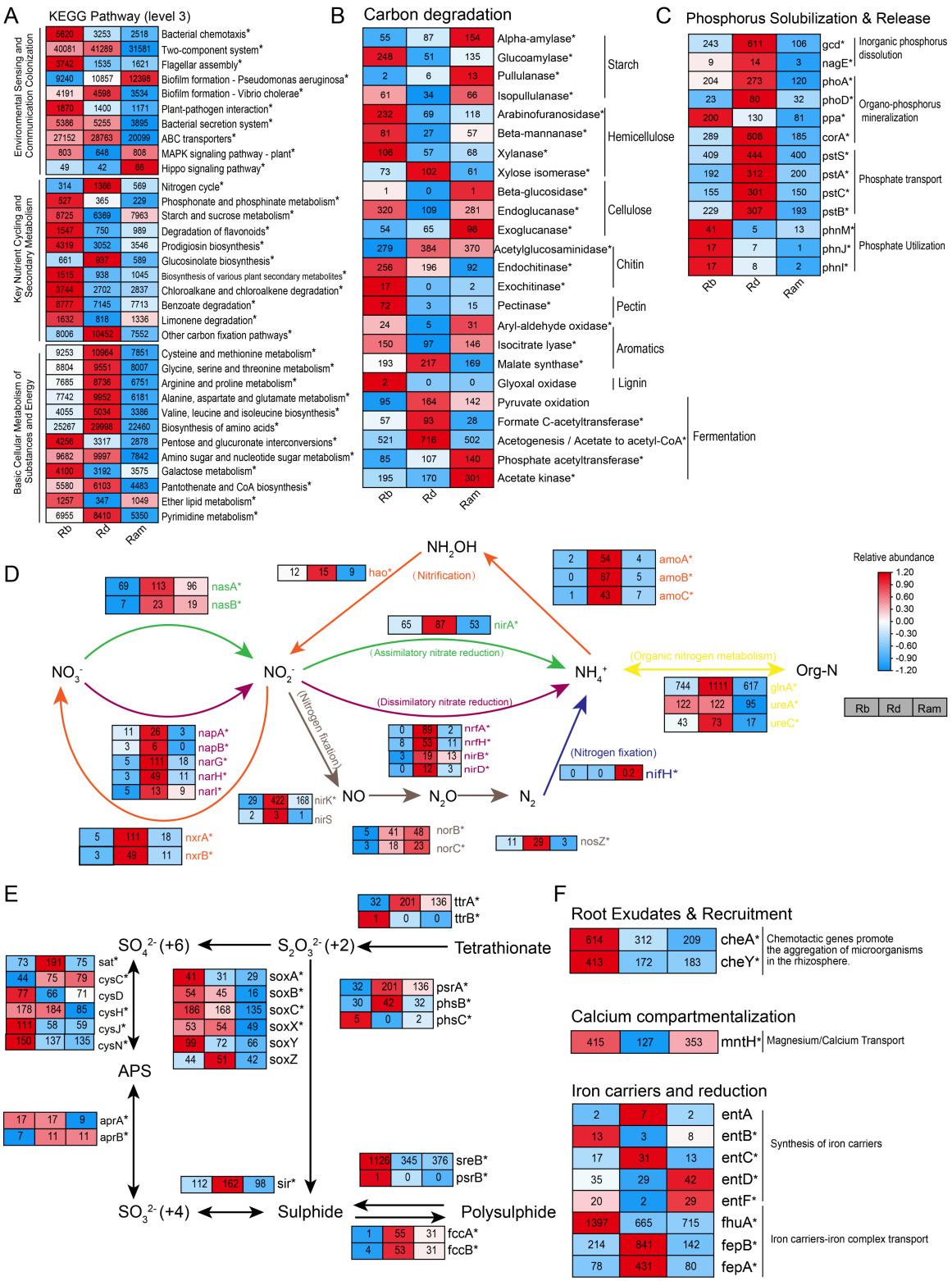


Figure 6

Rhizosphere metagenomic functions across three contrasting habitat soils. (A) The heatmap compares mean TPM values for the 33 KEGG level-3 pathways with the lowest P values across the three groups. Pathways are grouped into environmental sensing and communication, nutrient cycling and secondary metabolism, and basic cellular metabolism and energy. (B–F) Heatmaps and pathway schematics summarize annotations related to carbon degradation, phosphorus solubilization and release, nitrogen cycling, sulfur cycling, and environmental sensing, metal transport and iron acquisition, respectively. Cell values are mean TPM across three rhizosphere metagenomes per habitat, and the colour scale shows row-wise standardized DNA-derived TPM abundance. Asterisks indicate nominal two-tailed t-test comparisons at $P < 0.05$. Gene annotations and raw abundance data are provided in Additional file 6.

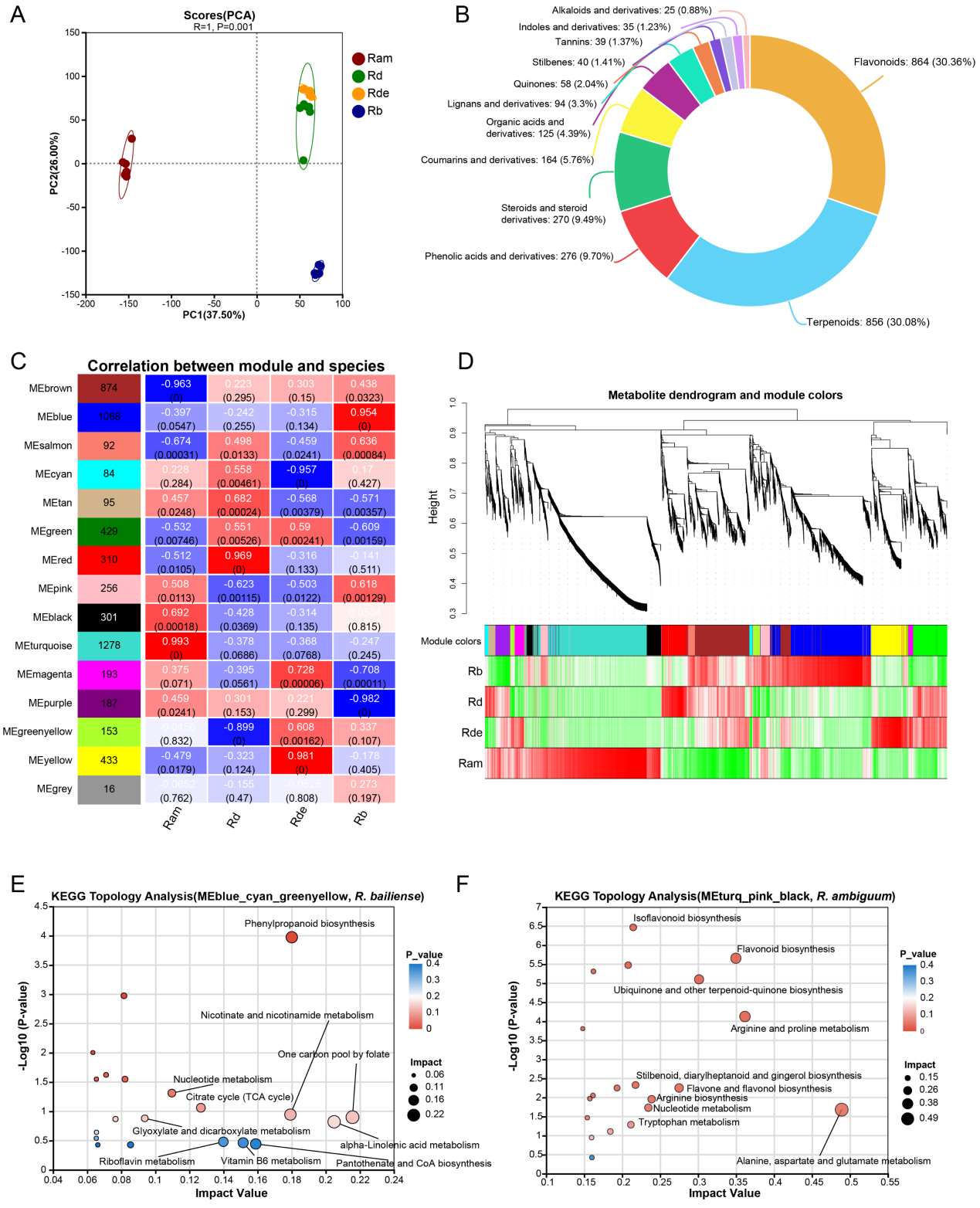


Figure 7

Metabolic profiles of four *Rhododendron* species across three typical habitats. (A) PCA reveals differences in metabolite composition among the four *Rhododendron* species. (B) Distribution and proportion of secondary metabolites identified through non-targeted metabolomics. (C) WGCNA analysis of the metabolic profiles of the four rhododendron species; the heatmap illustrates the correlation between modules and species. The column of numbers on the left indicates the number of metabolites in each module, while the data on the right for each group represents the correlation coefficient and significance P-value (in parentheses) between the module and the species. A larger absolute value indicates a stronger correlation; red indicates a positive correlation, and blue indicates a negative correlation. (D) A dendrogram of metabolites and a heatmap showing their correlation with modules. This figure illustrates the correlation between metabolites within a module and the four species. The top section shows the hierarchical clustering tree of metabolites, the middle section

displays the modules to which the metabolites belong, and the bottom section presents a heatmap of the correlations between metabolites within the module and the four species. Each row represents a species, and each column represents a metabolite within the module; colors indicate the strength of the correlation: red indicates a positive correlation, and green indicates a negative correlation. (E) KEGG Topology analysis of the MEblue + MEcyan + MEgreenyellow module (corresponding to the major dominant metabolites of *R. bailiense*). (F) KEGG Topology analysis of the MEturquoise + MEpink + MEblack module (corresponding to the major dominant metabolites of *R. ambiguum*). KEGG topology analysis reveals the classification of major dominant metabolites in *R. bailiense* and *R. ambiguum*. *R. delavayi* and *R. decorum* are two species inhabiting the same habitat. Abbreviations in the figure: Ram, *R. ambiguum*; Rb, *R. bailiense*; Rd, *R. delavayi*; Rde, *R. decorum*.

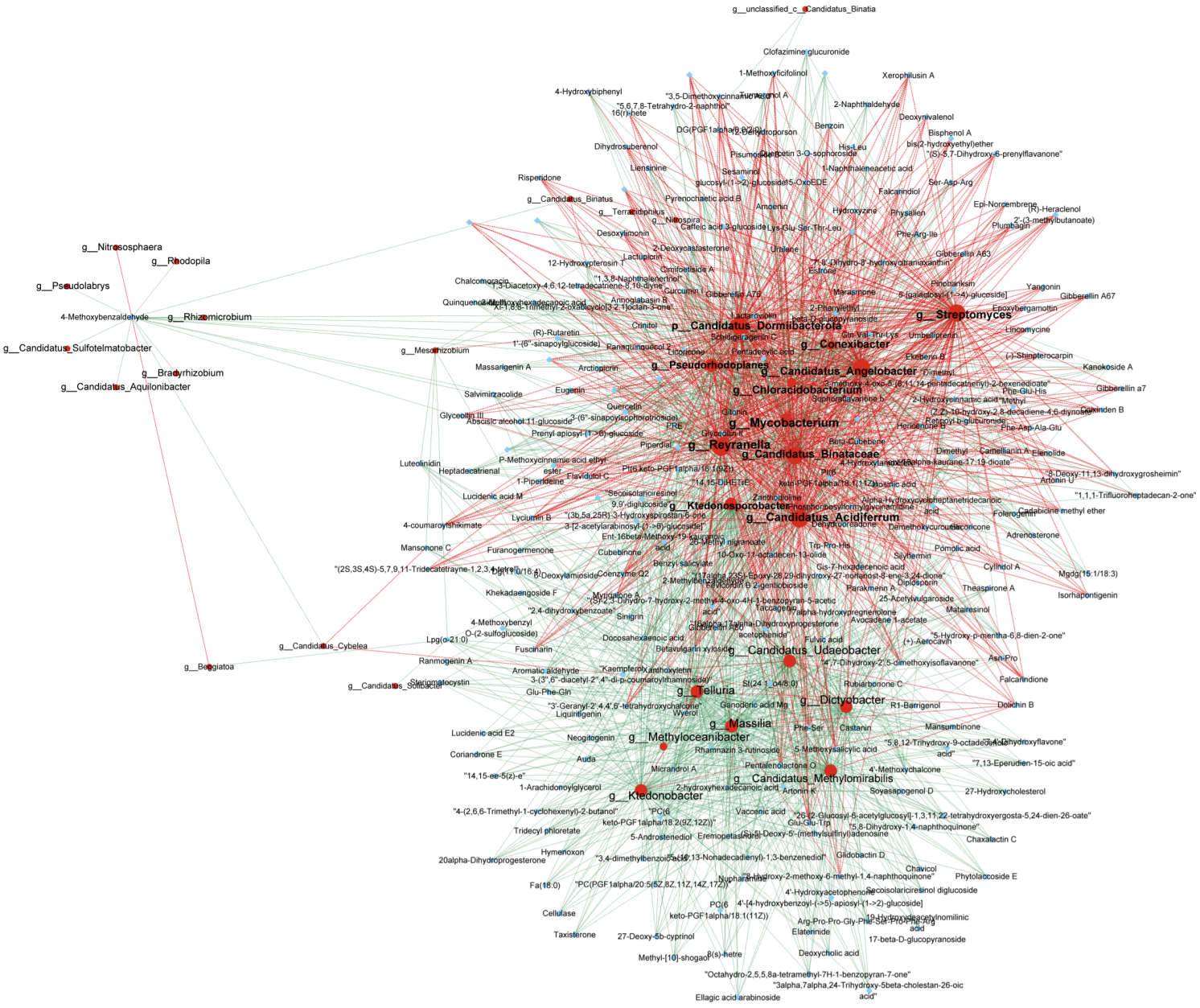


Figure 8

Cross-domain co-occurrence and association network between *Rhododendron*-specific core metabolites and rhizosphere microorganisms. Based on Spearman's rank correlation analysis, this figure illustrates the topological associations between representative dominant metabolites of *R. bailiense*, *R. delavayi*, and *R. ambiguum* and core rhizosphere microbial genera. Red nodes represent microbial genera in the microbiome network, while blue nodes represent host metabolites. Connections indicate retained correlations ($|\rho| > 0.6$ and nominal two-sided $P < 0.05$); red and green lines denote positive and negative correlations, respectively. The network is presented as a hypothesis-generating map of candidate metabolite–microorganism links. Please refer to Additional file 8 for the raw data.

Supplementary Files

This is a list of supplementary files associated with this preprint. Click to download.

- TableS1S121.xlsx
- DataS1S51.7z
- Supportinginformation1BMC.pdf